Astron. Astrophys. 247, 183–201 (1991)

ASTRONOMY AND ASTROPHYSICS

High resolution observations of interstellar Na I and Ca II towards the Scorpio-Centaurus association

I.A. Crawford

Department of Physics and Astronomy, University College London, Gower Street, London WC1E 6BT, United Kingdom

Received October 23, accepted December 18, 1990

Abstract. High-resolution observations (3.6 km s^{-1} FWHM) of interstellar Na I and Ca II towards 28 stars in the direction of the Sco-Cen association are presented. The observed velocity structure, velocity dispersions, column densities and Na I/Ca II ratios are discussed. Of the 58 identified velocity components (towards 23 stars), 46 (or 79%) were found to have negative LSR velocities. This is in agreement with previous results, and indicates a general outflow from the Sco-Cen association. By fitting an expanding shell model to the observed velocities an expansion velocity of 7 km s^{-1} was obtained. If the further assumption is made that only one component per star arises in such a shell, the best-fitting expansion velocity was found to be 9 km s^{-1}. In the latter case the remaining components were variously identified (depending on their velocities and Na I/Ca II ratios) as belonging to either: (i) relatively dense gas associated with the ρ Oph and Lupus dark clouds; (ii) low velocity material in the interior of the main Sco-Cen shell; (iii) local, low density, gas which forms a precursor to the main shell; and (iv) positive velocity gas which may exist beyond the bulk of the association.

Key words: Sco-Cen association – interstellar medium: bubbles – solar neighbourhood

1. Introduction

The Scorpio-Centaurus association is the closest OB association to the solar system. It occupies the galactic longitude range $290° \lesssim l \lesssim 360°$ (Blaauw 1964), i.e. almost the whole fourth galactic quadrant, and contains $\gtrsim 230$ stars mostly of spectral type B (e.g. de Geus, et al. 1989, and references therein). Blaauw (1964) identified three subgroups within the Sco-Cen association with the approximate longitude ranges as follows: Lower Centaurus – Crux (LCC; 292° to 312°), Upper Centaurus – Lupus (UCL; 312° to 341°), and Upper Scorpius (US; 341° to 2°). The upper Scorpius subgroup is also known as the Scorpius OB2 association (Blaauw 1964; Humphreys 1978). The Sco-Cen association lies along the plane of Gould's Belt, which is inclined to the galactic plane by about 20 degrees (Stothers & Frogel 1974), as a result of which the Upper Scorpius subgroup has a galactic latitude of about +20°, while the Lower Centaurus – Crux subgroup straddles the galactic plane. Jones (1971) obtained astrometric distances of 130, 140 and 160 pc (all plus or minus about 20 pc) for the LCC, UCL and US subgroups, respectively, and these distances are in good agreement with those obtained photometrically by de Geus et al. (1989; cf. their Table 5). The subgroups have rather different ages; de Geus et al. obtained nuclear ages in the range 11–12 million years (LCC), 14–15 million years (UCL), and 5–6 million years (US).

In the present work we present high-resolution observations of interstellar Na I D_2 and Ca II K lines towards twenty-eight B stars in the direction of the Sco-Cen association. Table 1 lists the basic observational data for these stars. The tabulated V magnitudes, spectral types and projected rotational velocities ($v \sin i$) have been taken from the Bright Star Catalogue (Hoffleit & Jaschek 1982). For all stars except κ Vel and σ Cen, the reddenings and distances have been taken from the recent photometry of de Geus et al. (1989, assuming $R = 3.1$ for the conversion of A_V to E_{B-V}). All the stars except κ Vel and σ Cen are listed by de Geus et al. as proper motion members of the association; σ Cen is listed as a member by Bertiau (1958), and although κ Vel seems not to be a member, it was observed because it lies in a similar region of space. For these two stars, the reddenings and distances were estimated from their spectral types and the intrinsic colours of Deutschman et al. (1976). The last column of Table 1 gives the difference between the LSR and heliocentric radial velocities for each line of sight; this quantity should be added to the LSR velocities in order to obtain heliocentric values.

Figure 1a shows the positions of the observed stars projected onto the galactic plane. The dashed circles in Fig. 1 represent the LCC, UCL and US H I shells described by de Geus (1991), and which will figure prominently in the ensuing discussion. Also marked in Fig. 1 are the locations of the nearby dark clouds which occur in this region of space, taken from the extensive survey of Dame et al. (1987). The clouds are represented by circles, the diameters of which correspond to the longitude range occupied by each cloud on the sky. It will be seen that these dark clouds occur beyond the bulk of the Sco-Cen association, where they form a 'wall' of denser material. However, three of the stars observed here (ω^1 Sco, χ Oph and 48 Lib) lie beyond this wall; moreover, the interstellar spectra indicate that the stars 1 Sco and HD 148703 (and possibly also 2 Sco and θ Oph) may also lie beyond these clouds, and hence at greater distances than indicated in Fig. 1a. Figure 1b shows the positions of the observed stars plotted in galactic coordinates. The areas of sky occupied by the dark clouds discussed above are indicated by rectangles (the sides of which connect the ranges of l and b listed for each cloud by Dame et al. (1987)). The three stars that are placed beyond the dark clouds by the photometry of de Geus et al. (1989) are specially indicated although, as noted above, several other stars may also lie beyond the dark clouds. The LCC and US shells are drawn

Table 1. Observational data for the stars observed. The reddenings and distances are from de Geus et al. (1989), except for κ Vel and σ Cen (indicated by parentheses) which have been estimated from the spectral types (see text). The quantity in the last column should be added to the LSR velocities in order to obtain heliocentric values

HD	Name	l	b	V	Sp. type	$v \sin i$ (km s^{-1})	E_{B-V}	d (pc)	$\Delta v_{\mathrm{LSR,hel}}$ (km s^{-1})
81188	κ Vel	275.9	−3.5	2.5	B2 IV-V	49	(0.08)	(102)	+14.6
103079		296.7	−3.1	4.9	B4 V	57	0.03	100	+9.5
105435	δ Cen	296.0	+11.6	2.6	B2 IVne	181	0.13	171	+7.5
105937	ρ Cen	296.8	+10.0	4.0	B3 V	140	0.00	83	+7.6
106490	δ Cru	298.2	+3.8	2.8	B2 IV	194	0.02	153	+8.1
108483	σ Cen	299.1	+12.5	3.9	B2 V	245	(0.07)	(173)	+6.5
110956		302.2	+6.4	4.7	B3 V	66	0.02	114	+6.6
116087		306.7	+1.7	4.5	B3 V	241	0.02	103	+5.9
118716	ϵ Cen	310.2	+8.7	2.3	B1 III	159	0.02	168	+3.8
120324	μ Cen	314.2	+19.1	3.0	B2 IV-Ve	175	0.01	145	+1.1
121743	ϕ Cen	316.0	+19.1	3.8	B2 IV	126	0.01	157	+0.6
125823		321.6	+20.0	4.4	B7 IIIp	2	0.01	135	−1.3
130807	o Lup	324.9	+14.1	4.3	B5 IV	84	0.01	102	−1.5
132058	β Lup	326.3	+13.9	2.7	B2 III	127	0.02	156	−1.9
132200	κ Cen	326.9	+14.8	3.1	B2 IV	28	0.01	118	−2.2
133955	λ Lup	326.8	+11.1	4.1	B3 V	166	0.01	104	−1.7
138690	γ Lup	333.2	+11.9	2.8	B2 IV	393	0.02	110	−3.8
138769		331.0	+8.8	4.5	B3 IVp	101	0.00	132	−2.7
141637	1 Sco	346.1	+21.7	4.6	B3 V	300	0.15	67	−8.7
142114	2 Sco	346.9	+21.6	4.6	B2.5 Vn	308	0.11	112	−8.9
142669	ρ Sco	344.6	+18.3	3.9	B2 IV-V	156	0.02	138	−8.0
142983	48 Lib	356.4	+28.6	4.9	B5 IIIpe	393	0.04	673	−11.9
143699		339.1	+10.4	4.9	B6 IV	201	0.01	122	−5.5
144470	ω^1 Sco	352.8	+22.8	4.0	B1 V	142	0.02	183	−10.6
148184	χ Oph	357.9	+20.7	4.4	B2 IVpe	134	0.57	263	−11.8
148703		345.9	+9.2	4.2	B2 III-IV	90	0.06	154	−7.4
151890	μ^1 Sco	346.1	+3.9	3.1	B1.5 V	239	0.03	147	−6.8
157056	θ Oph	0.5	+6.6	3.3	B2 IV	35	0.03	130	−11.2

in Fig. 1b (the UCL shell is too large to be shown), and the plane of Gould's Belt is indicated (Stothers & Frogel 1974).

It is hoped that the Na I and Ca II data presented here will complement a number of recent studies of the distribution of local interstellar material. In particular, Paresce (1984) has tabulated the H I column densities towards 12 of the stars included in this work, Franco (1990) has performed a detailed study of the interstellar colour excesses found in the direction of Sco-Cen, and de Geus (1991) has discussed the interaction of stars and interstellar matter in the vicinity of the association. Readers may find it of interest to compare the data reported by these authors with the present interstellar absorption line data.

2. Observations and reductions

All the observations described here were obtained with the coudé échelle spectrograph of the Mt Stromlo 74-inch telescope during 1989 May and June. The spectrograph was used with the 130-inch focal length camera, yielding a dispersion of 0.53 Å mm^{-1} at the Na D2 (5889.950 Å) line and 0.35 Å mm^{-1} at the Ca II K (3933.663 Å) line. These dispersions result in a spectral coverage of 6 Å at Na D and 4 Å at Ca K. The adopted slit width was 300 μm, which corresponds to a velocity resolution (FWHM) of 3.6 km s^{-1}. This resolution was determined both by theoretical calculations (Crawford et al. 1987), and by measurements of the width of Th–Ar comparison arc lines.

Full details of the data calibration and reduction of similar Mt Stromlo coudé spectra have been given previously by Crawford et al. (1989), and will not be repeated here. It is, however, worth reiterating that only two lines from the Th–Ar lamp fell within the very narrow wavelength intervals sampled by the detector, necessitating the use of a linear wavelength interpolation. Analysis of Th–Ar spectra obtained with the 32-inch camera (which results in four-fold increase in spectral coverage, and therefore in more lines falling on the detector) revealed that this linear interpolation introduces an error of $\lesssim$2 mÅ (0.15 km s^{-1}) at Na D, and $\sim$4 mÅ (0.3 km s^{-1}) at Ca K. After wavelength calibration, the observed wavelengths were converted to the LSR velocity frame, assuming a solar motion of 20 km s^{-1} towards $\alpha = 18^{\mathrm{h}}$, $\delta = +30°$ (Allen 1973).

Atmospheric water lines occur in the region of the Na D lines (see, e.g., Hobbs 1978) and, as described by Crawford et al. (1989), these were divided out of the observed spectra. In this work, the atmospheric spectrum was taken to be given by the spectrum of γ Lup, since no interstellar Na absorption was discernable towards this star. Small ($\lesssim$10%) variations in the strength of the

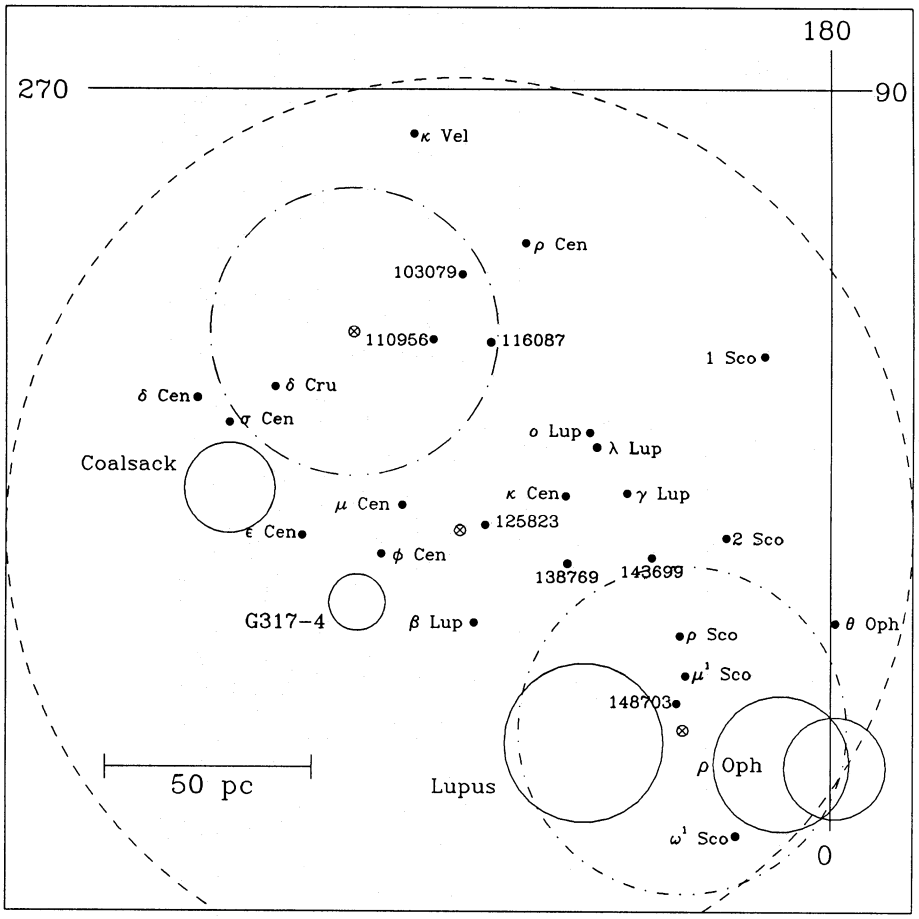

Fig. 1a. A projection of the observed stars onto the galactic plane; the sun lies at the origin of the galactic coordinates. The stellar distances have been taken from the photometry of de Geus et al. (1989); but note that the interstellar spectra indicate that the stars 1 Sco, and HD 148703, and possibly also 2 Sco and θ Oph, actually lie at greater distances than indicated (cf. Sects. 7.3 and 7.4). The stars 48 Lib and χ Oph are too distant to be plotted on this scale. The *dashed circles* indicate the extent of the LCC, UCL and US H I shells discussed by de Geus (1991), the centres of which are marked by ⊗. The remaining *circles* (drawn with solid lines) show the positions of nearby dark clouds, the names of which are indicated; the distances and sizes of these clouds been taken from Dame et al. (1987)

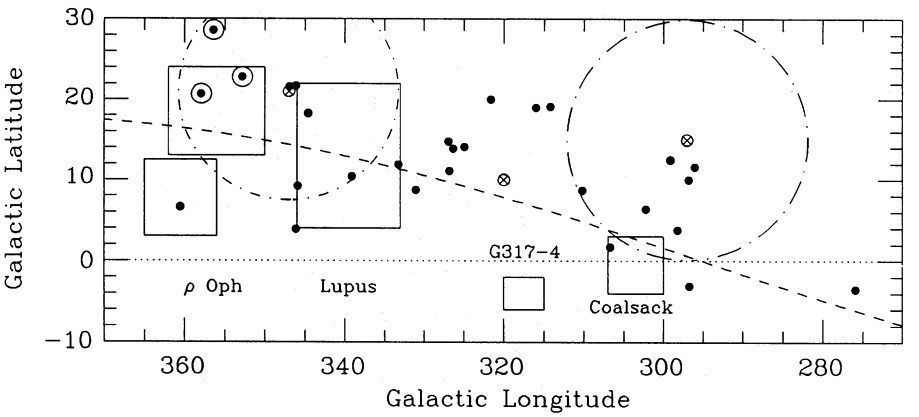

Fig. 1b. The observed stars plotted in galactic coordinates. The extent of the US and LCC shells, and the nearby dark clouds, are also plotted. The stars 48 Lib, ω^1 Sco and χ Oph, which are placed beyond the dark clouds by the photometry of de Geus et al. (1989), are indicated by ⊙ *symbols*. The *dotted line* marks the galactic plane, and the *dashed line* marks the plane of Gould's Belt (Stothers & Frogel 1974)

atmospheric lines were found between the different spectra reported here, and these were allowed for by scaling the optical depth of the adopted atmospheric spectrum appropriately before division. The observed spectra are shown in Fig. 2. The success of the atmospheric correction procedure is apparent from the fact that all the water lines which are clear of the interstellar lines have been satisfactorily removed. (The interested reader will find the positions of these lines indicated in Fig. 1 of Hobbs 1978.)

3. The stellar lines

When interpreting interstellar Na D and Ca K absorption lines it is necessary to consider the extent to which these lines are also present in the spectrum of the background star. The main concern is the strength of the stellar K line, which Hobbs (1973) has shown may have a equivalent width as large as 80 mÅ even in stars as early as B2. In order to quantify the increase in the stellar equivalent width for cooler B stars, Crawford (1990) made use of the Kurucz (1979) LTE model atmospheres to calculate the expected K line equivalent width as a function of stellar temperature. For the range of spectral types of interest here it was found that the stellar K line equivalent width increased from about 70 mÅ (B2) to about 200 mÅ (B7) for stars of solar composition (cf. Fig. 1 of Crawford 1990).

In cases where an obvious stellar line was found, it has been fitted with a theoretical rotational profile. These profiles are

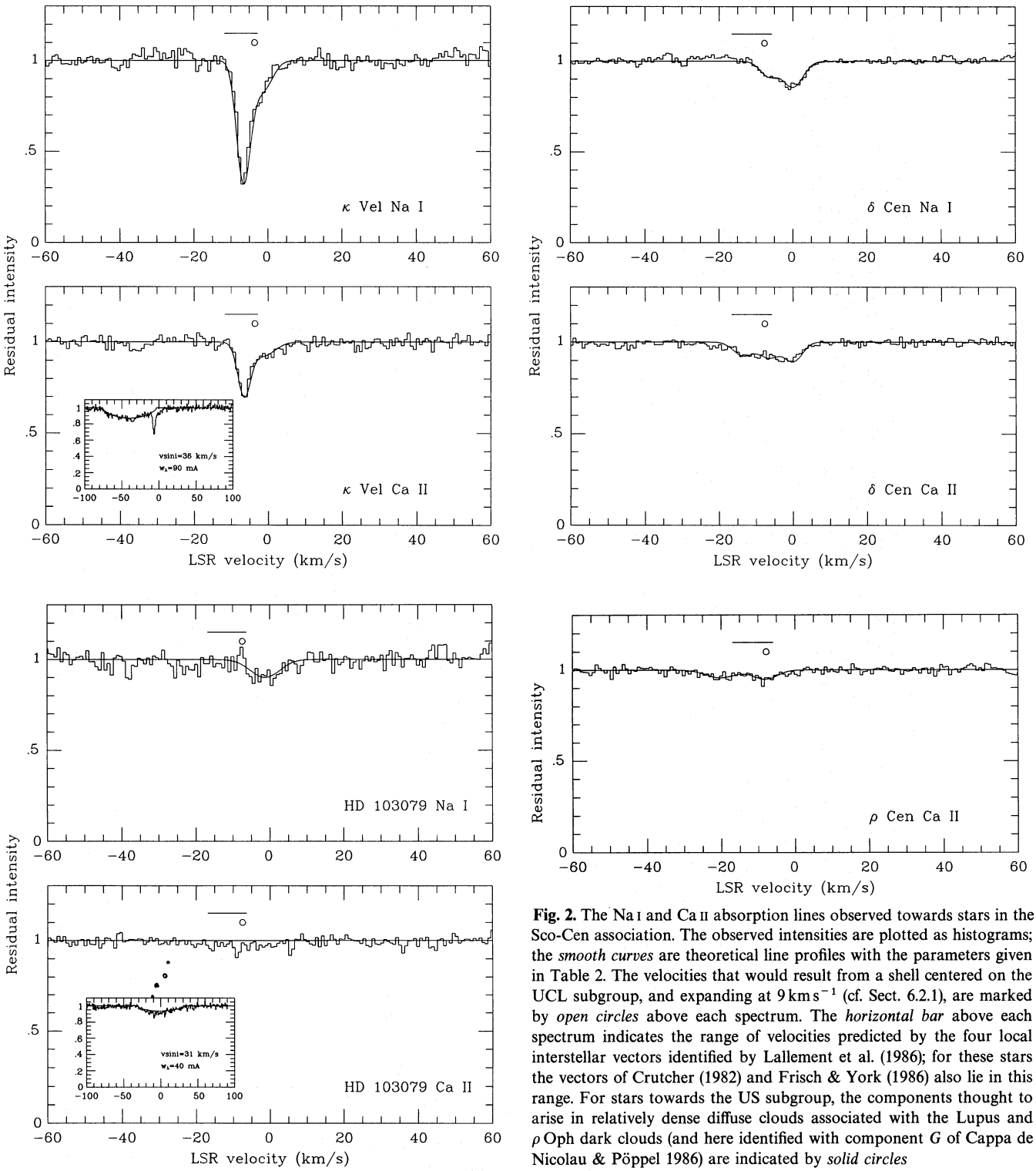

Fig. 2. The Na I and Ca II absorption lines observed towards stars in the Sco-Cen association. The observed intensities are plotted as histograms; the *smooth curves* are theoretical line profiles with the parameters given in Table 2. The velocities that would result from a shell centered on the UCL subgroup, and expanding at 9 km s^{-1} (cf. Sect. 6.2.1), are marked by *open circles* above each spectrum. The *horizontal bar* above each spectrum indicates the range of velocities predicted by the four local interstellar vectors identified by Lallement et al. (1986); for these stars the vectors of Crutcher (1982) and Frisch & York (1986) also lie in this range. For stars towards the US subgroup, the components thought to arise in relatively dense diffuse clouds associated with the Lupus and ρ Oph dark clouds (and here identified with component *G* of Cappa de Nicolau & Pöppel 1986) are indicated by *solid circles*

shown as insets in Fig. 2, and the inferred equivalent width and $v \sin i$ are indicated. The equivalent widths are generally in agreement with those expected from the spectral types. The inferred values of $v \sin i$ may be compared with those given in Table 1, where it will be seen that for two stars (HD 103079 and *o* Lup) the rotational velocities found here are significantly smaller than given by the *Bright Star Catalogue*, but that for the other stars the agreement is fairly good.

In addition to the Ca K line, there is an S II line at 3933.29 Å (28 km s^{-1} to the blue of the K line) which may occur in the spectra of B stars. The models discussed by Crawford (1990) suggest that this line will reach a maximum equivalent width of about 30 mÅ at a spectral type of B3. In the present work evidence for this line was found for HD 110956 and HD 125823; in both cases it was found that the presence of S II helped explain the broad and asymmetric absorption found for these stars. Two

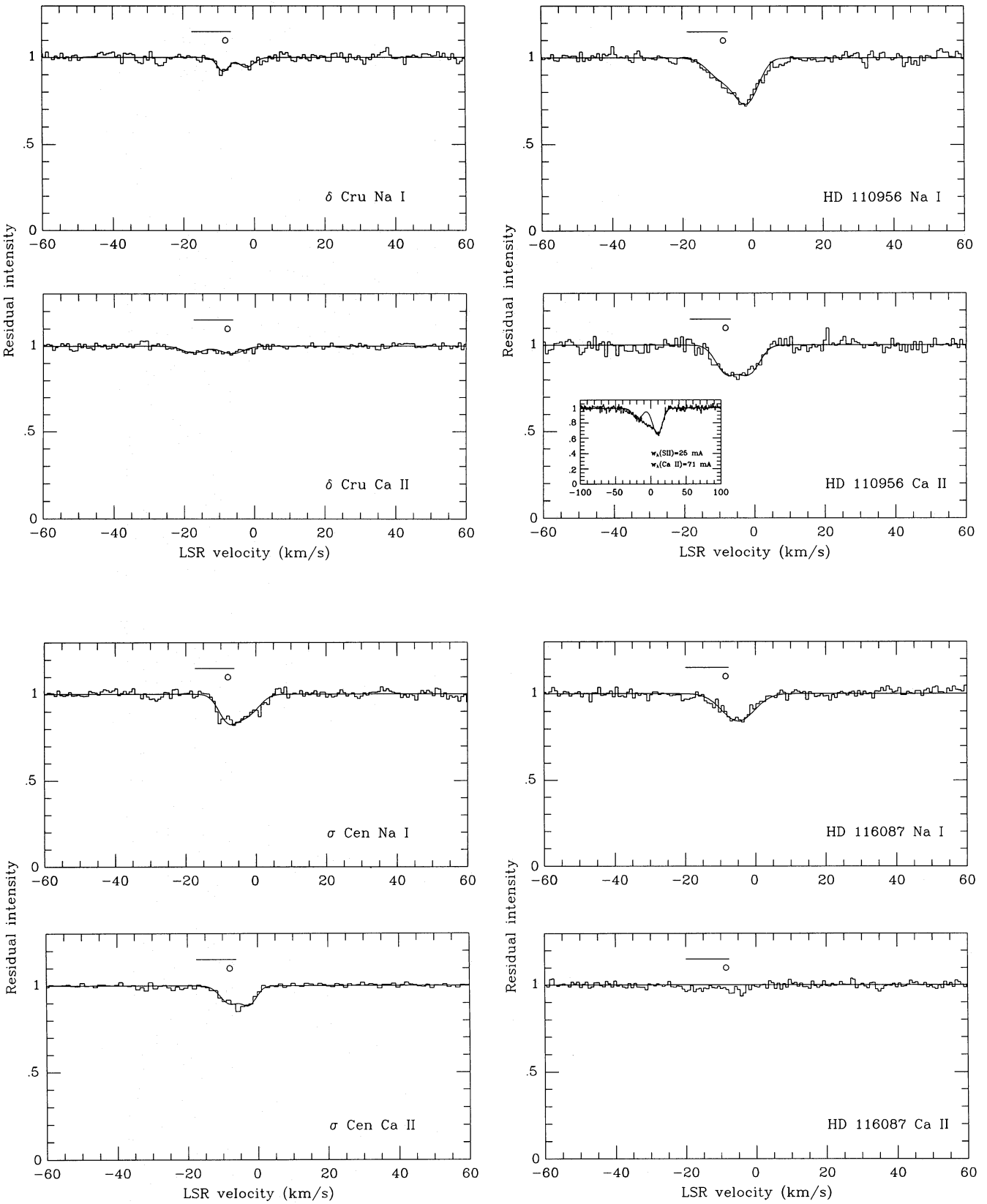

Fig. 2 (continued)

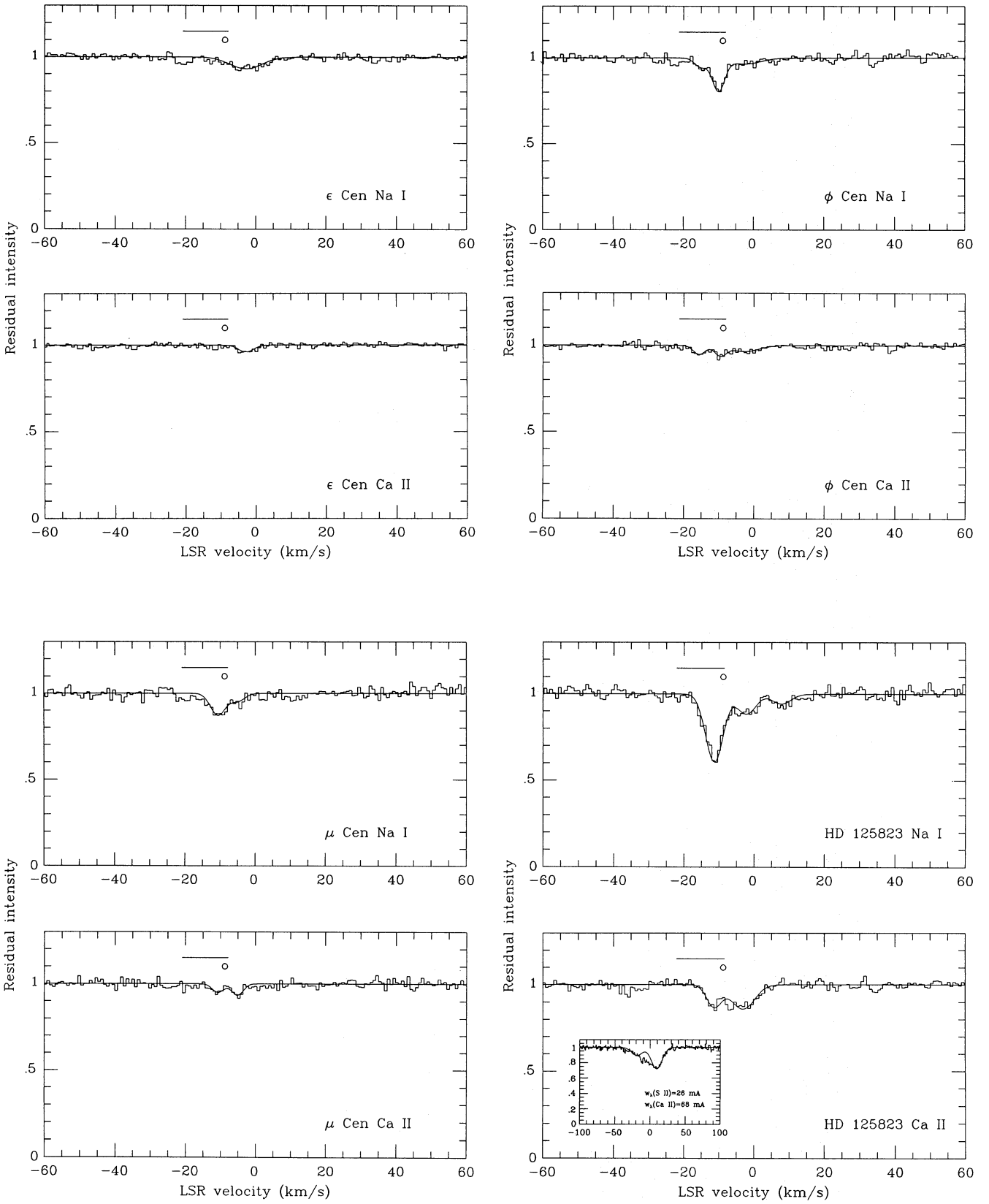

Fig. 2 (continued)

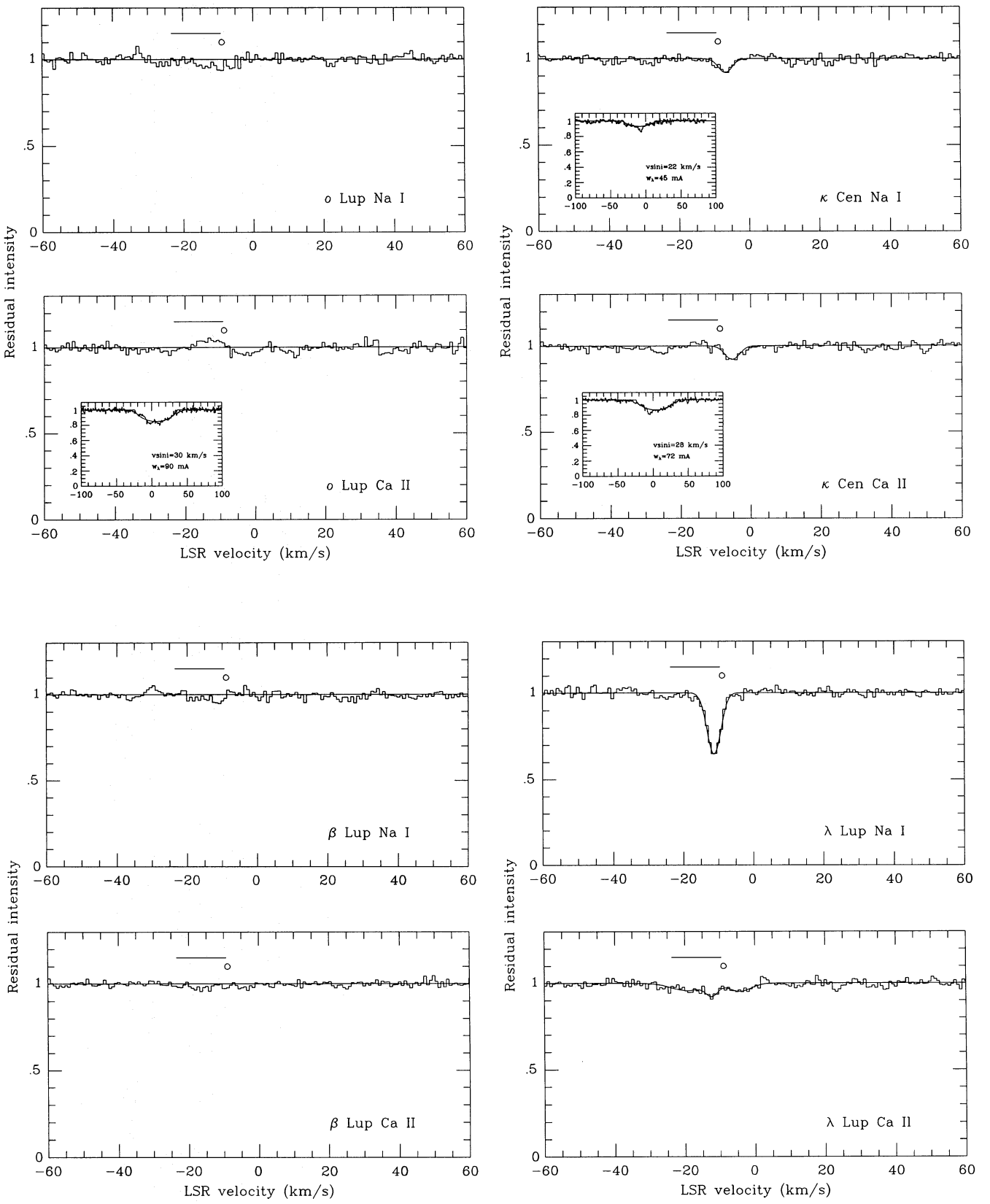

Fig. 2 (continued)

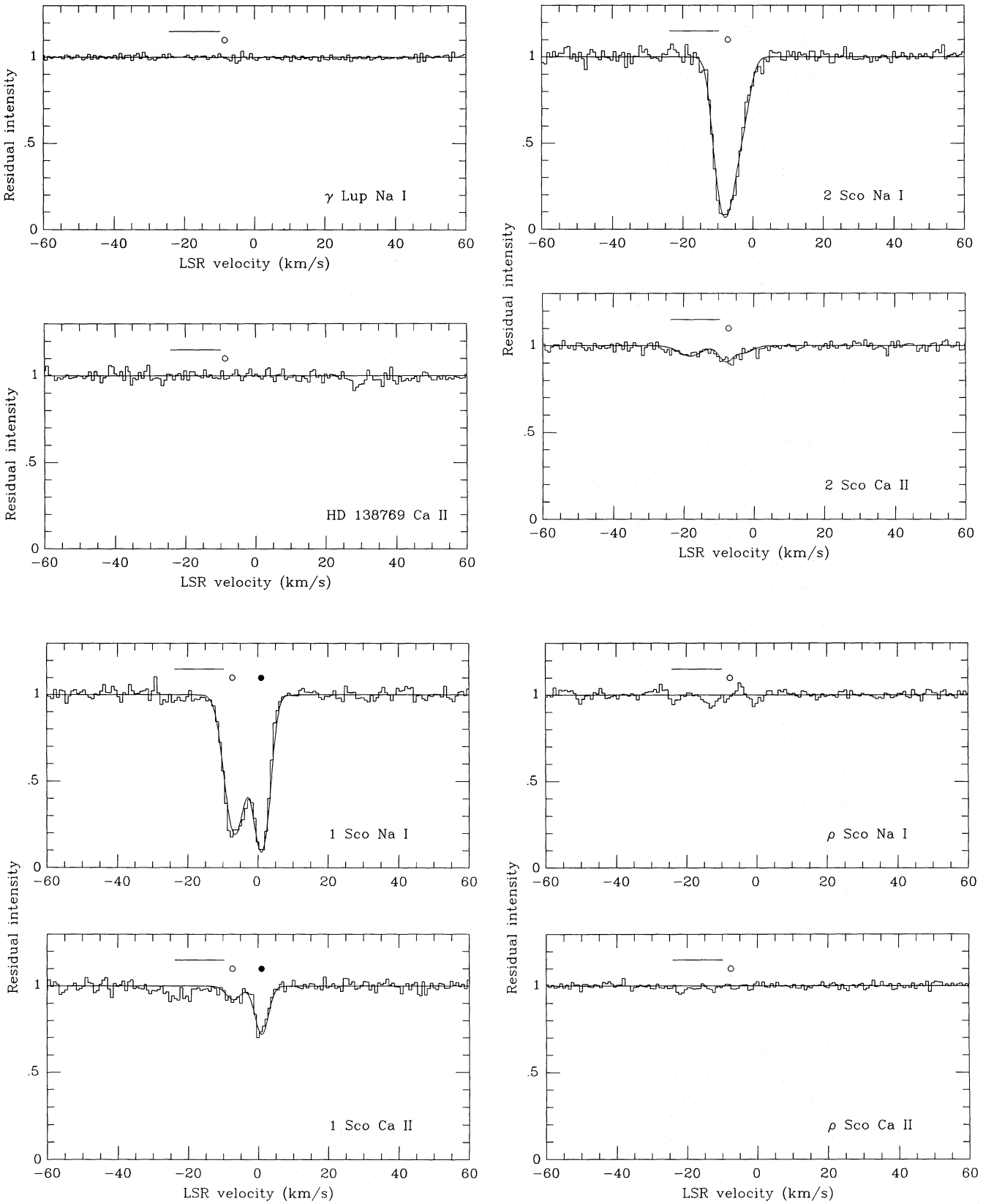

Fig. 2 (continued)

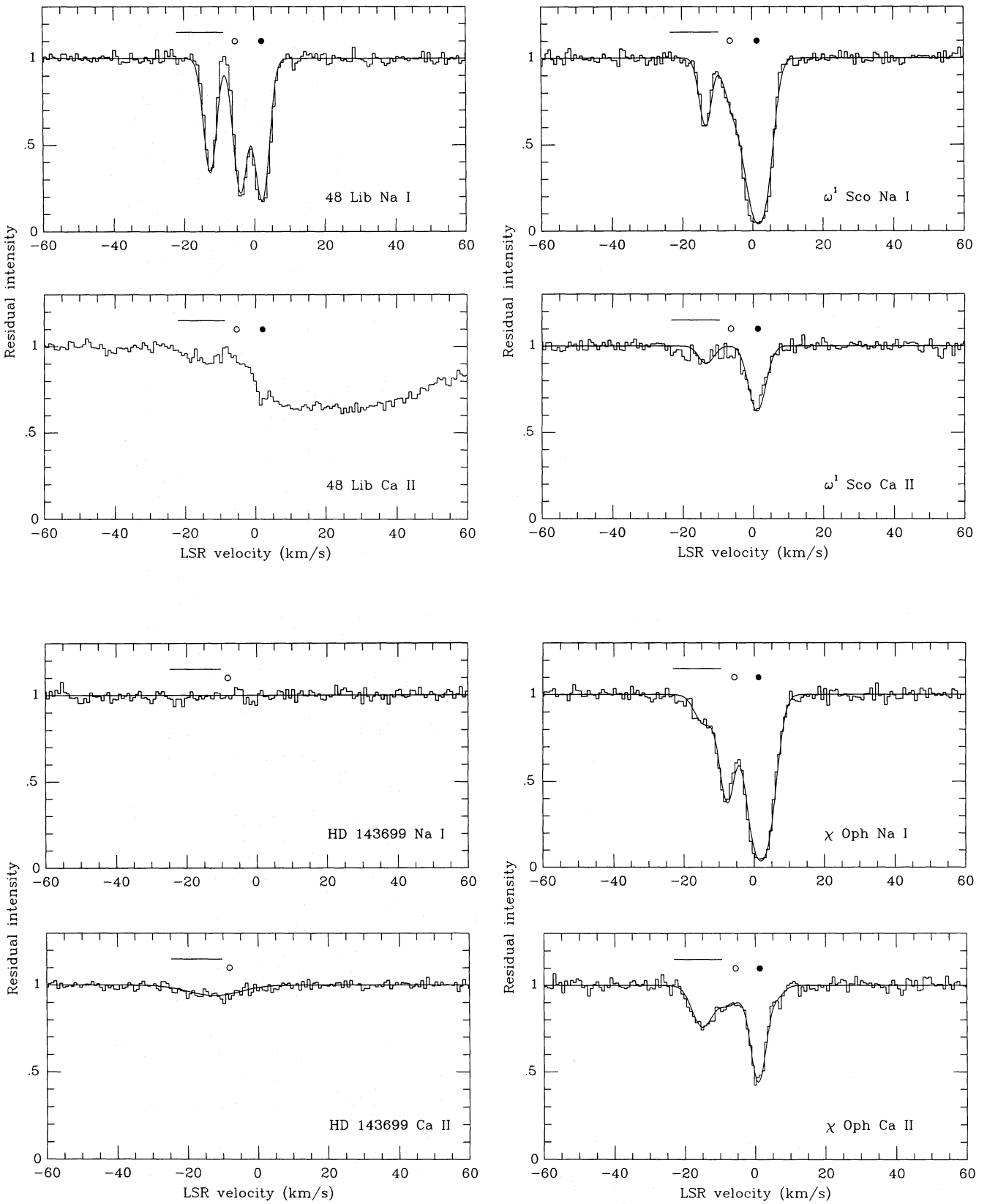

Fig. 2 (continued)

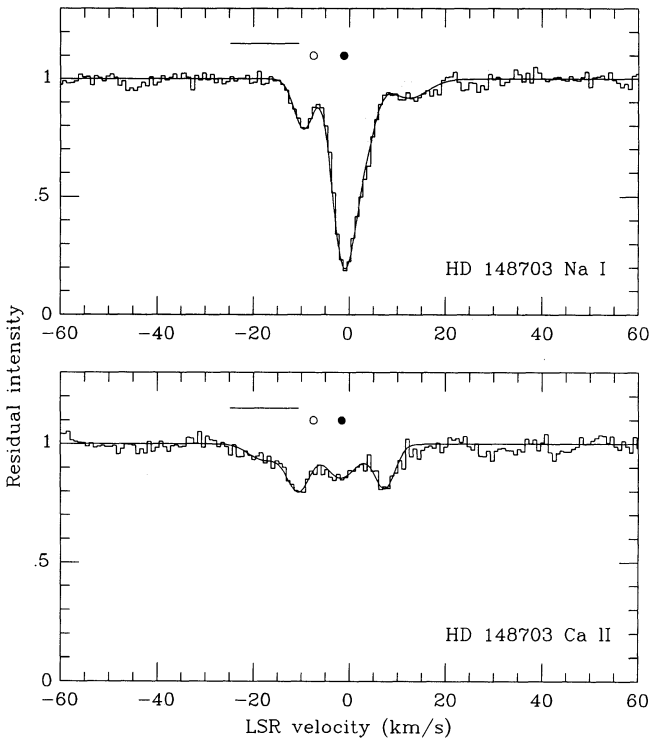

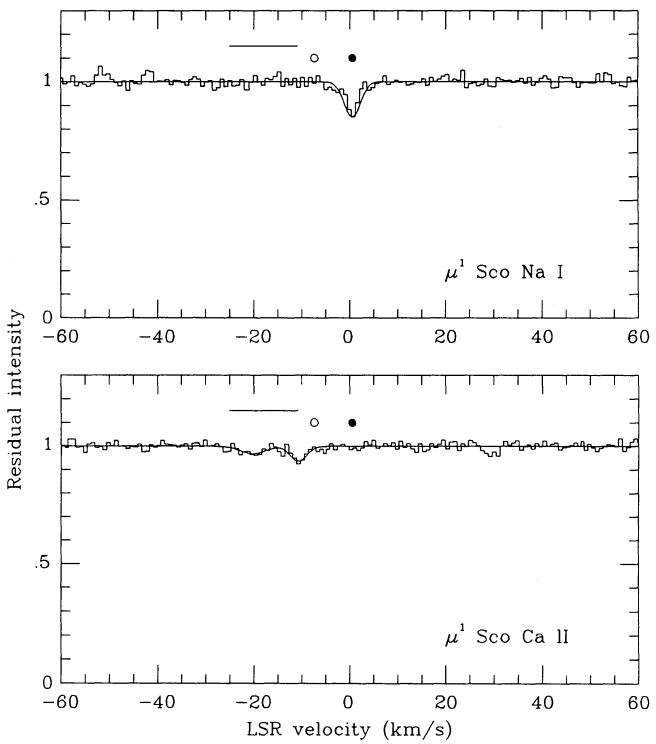

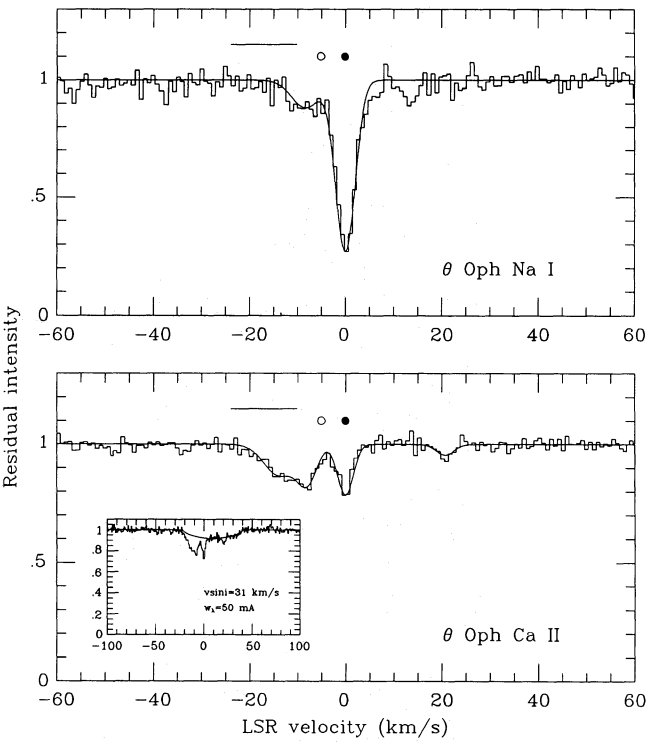

Fig. 2 (continued)

component Gaussian fits to these profiles are shown as insets to the appropriate plots in Fig. 2. For HD 110956 (B3 V) the S II equivalent width (25 mÅ) agrees well with that expected from the spectral type; in the case of HD 125823 (B7 IIIp), the inferred equivalent width is a factor of three larger than might be expected for a normal star of this type, but this star is classed as peculiar.

In contrast to the Ca K line, the stellar Na D line is expected to be very weak throughout the class of B stars (being $\lesssim 20$ mÅ for stars earlier than B7). Of greater importance is the C II line at 5889.78 Å (only 9 km s^{-1} to the blue of the D2 line), which is expected to reach a maximum equivalent width of about 80 mÅ at a spectral type of B2 (cf. Fig. 2 of Crawford 1990). Convincing evidence for this line was found only in the case of κ Cen; the inferred $v \sin i$ agrees well with that found for the stellar K line towards this star, although the equivalent width (45 mÅ) is about half that expected from the spectral type.

In all cases where stellar lines were identified, the profiles of these were divided into the observed spectra. Only in one case (Ca II towards 48 Lib) was broad, clearly non-interstellar, absorption found that could not be easily ascribed to a stellar line. In this case the absorption, which extends over about 80 km s^{-1}, is much narrower than the rotational velocity of the star (393 km s^{-1}). However, 48 Lib is a well known shell star, and it is possible that the feature observed here is circumstellar in origin; weak interstellar Ca K lines can be seen in its blue wing, at the same velocities as the much stronger interstellar sodium lines.

4. Line profile analysis and column densities

Once the spectra had been corrected for atmospheric and stellar absorption, the analysis proceeded by means of line profile fitting. The theoretical profiles were calculated using the DIPSO program (Howarth & Murray 1988) on the UCL *Starlink* node, and followed the procedure described by Crawford et al. (1989). The results of this analysis are given in Table 2, which lists the LSR radial velocity, $v_{\rm lsr}$; column density, N; and velocity dispersion, b, deduced for each velocity component. Theoretical profiles with these parameters are shown (after convolution with the instrumental profile) superimposed on the observed spectra in Fig. 2. The adopted oscillator strengths were 0.655 for Na D2 and 0.688

Table 2. Equivalent widths, w_λ (mÅ); LSR velocities, v_{lsr} (km s^{-1}); velocity dispersions, b (km s^{-1}); and column densities, N (cm^{-2}), for the interstellar Na I D2 and Ca II K lines observed towards the Sco-Cen association. The equivalent widths are summed over all identified velocity components; the errors are 2σ values based on the continuum scatter and an assumed 4% zero level error. Δb and ΔN are the ranges of b and N that give acceptable fits to the observed profiles; for unresolved lines an upper limit is given under Δb, and the upper limit to N calculated for assumed values of $b = 0.30$ km s^{-1} for Na and 0.23 km s^{-1} for Ca, see text for discussion. For components identified in only one species, the column density upper limit for the other has been estimated from the equivalent width upper limit at that velocity, assuming a linear curve of growth. Components in Na and Ca are judged to correspond if they occur within 2 km s^{-1} of each other

Star	w_λ(Na I)	w_λ(Ca II)	Na I components					Ca II components				
			v_{lsr}	b	N	Δb	ΔN	v_{lsr}	b	N	Δb	ΔN
κ Vel	73 ± 7	22 ± 3	−6.6	1.0	8.0(11)	≤1.5	0.6–50(12)	−6.6	1.0	2.3(11)	≤2.0	2.0–30(11)
			−1.6	3.0	1.2(11)	≤4.0	1.0–2.0(11)	−1.6	4.0	9.0(10)	3.0–7.0	0.5–1.1(11)
103079	17 ± 5	≤6.5	−1.2	5.0	1.0(11)	4.0–6.0	0.8–1.3(11)	–	–	≤7.0(10)	–	–
δ Cen	31 ± 3	21 ± 2	–	–	≤1.0(10)	–	–	−13.5	3.0	7.0(10)	1.0–4.0	0.4–1.0(11)
			−6.5	2.5	5.0(10)	2.0–4.0	4.0–7.0(10)	−6.5	3.0	8.0(10)	1.0–5.0	0.5–1.0(11)
			0.0	3.0	1.0(11)	2.5–4.0	0.9–1.2(11)	0.0	2.5	9.0(10)	1.0–3.5	0.6–1.1(11)
ρ Cen	–	12 ± 2	–	–	–	–	–	−20.1	5.0	6.0(10)	3.0–8.0	3.0–9.0(10)
			–	–	–	–	–	−8.1	4.0	6.0(10)	2.0–7.0	0.3–1.0(11)
δ Cru	13 ± 3	10 ± 2	–	–	≤0.7(10)	–	–	−17.6	3.5	4.0(10)	2.0–5.0	3.0–5.0(10)
			−8.5	1.0	3.5(10)	≤2.0	3.0–4.5(10)	−6.6	4.0	5.0(10)	3.0–6.0	4.0–7.0(10)
			−1.9	2.0	3.0(10)	1.5–3.0	2.0–3.5(10)	–	–	≤2.0(10)	–	–
σ Cen	38 ± 4	16 ± 2	−8.0	3.0	1.0(11)	2.0–4.0	0.7–1.3(11)	−8.0	3.0	1.0(11)	2.0–3.5	0.7–1.2(11)
			−2.5	4.0	1.0(11)	3.0–5.0	0.7–1.1(11)	−2.5	3.0	8.0(10)	1.0–3.0	0.6–1.1(11)
110956	67 ± 6	31 ± 4	−8.6	5.0	1.2(11)	4.0–5.5	0.9–1.7(11)	−8.1	3.5	1.8(11)	3.0–4.5	1.5–2.1(11)
			−1.6	4.0	2.3(11)	3.0–5.0	1.8–2.9(11)	−1.6	3.5	1.8(11)	2.0–4.0	1.2–2.1(11)
116087	35 ± 4	4.1 ± 1.2	−4.9	6.0	1.9(11)	4.0–7.0	1.4–2.2(11)	−4.9	–	4.4(10)	–	3.1–5.7(10)
ϵ Cen	17 ± 2	3.0 ± 1.0	−2.8	6.0	8.0(10)	5.0–8.0	0.6–1.1(11)	−2.8	2.0	3.0(10)	1.0–4.0	2.5–4.5(10)
μ Cen	22 ± 3	5 ± 2	−10.6	2.0	7.0(10)	1.2–2.5	6.0–8.0(10)	−10.6	0.8	3.0(10)	≤1.0	2.0–4.0(10)
			−5.1	2.0	2.5(10)	≤2.5	2.0–3.0(10)	−5.1	0.8	4.0(10)	≤1.0	3.0–5.0(10)
ϕ Cen	25 ± 4	10 ± 2	−15.1	1.0	2.4(10)	≤2.0	2.0–3.2(10)	−15.6	1.0	3.2(10)	≤3.0	2.5–4.5(10)
			−10.1	1.0	9.5(10)	≤2.0	0.8–1.1(11)	−9.6	1.0	3.5(10)	≤3.0	3.0–4.0(10)
			−2.6	6.0	4.0(10)	4.0–9.0	3.0–5.0(10)	−2.6	5.0	4.8(10)	3.0–7.0	3.3–5.5(10)
125823	68 ± 8	23 ± 3	−11.4	2.5	3.0(11)	2.0–3.5	2.5–3.5(11)	−11.4	2.0	1.0(11)	≤3.0	0.8–1.1(11)
			−2.2	3.0	8.0(10)	2.5–4.0	0.6–1.1(11)	−3.2	4.0	1.7(11)	3.5–6.0	1.3–2.2(11)
			+7.8	3.0	3.8(10)	≤5.0	3.2–5.0(10)	–	–	≤1.4(10)	–	–
o Lup	≤9.0	≤8.0	–	–	≤4.5(10)	–	–	–	–	≤8.5(10)	–	–
β Lup	≤6.5	≤3.0	–	–	≤3.2(10)	–	–	–	–	≤3.2(10)	–	–
κ Cen	6.7 ± 1.8	5.9 ± 1.3	−6.8	1.5	4.0(10)	1.0–2.0	3.2–4.5(10)	−5.3	2.0	6.0(10)	1.0–3.0	5.0–8.0(10)
λ Lup	34 ± 4	14 ± 2	–	–	≤2.0(10)	–	–	−19.3	6.0	7.0(10)	4.0–10.0	0.5–1.2(11)
			−11.3	1.5	2.2(11)	≤2.0	1.9–3.5(11)	−12.3	1.0	4.0(10)	≤2.0	2.0–6.0(10)
			–	–	≤1.5(10)	–	–	−4.3	4.0	5.5(10)	3.0–6.0	4.0–7.0(10)
γ Lup	≤1.4	–	–	–	≤0.7(10)	–	–	–	–	–	–	–
138769	–	≤1.5	–	–	–	–	–	–	–	≤1.6(10)	–	–
1 Sco	218 ± 18	21 ± 3	−6.7	2.7	1.1(12)	2.2–3.0	1.0–1.3(12)	−7.0	2.0	6.0(10)	1.0–4.0	4.0–9.0(10)
			+1.0	1.6	2.4(12)	0.6–2.3	0.14–20(13)	+1.0	1.5	2.3(11)	≤2.0	2.0–30(11)
2 Sco	167 ± 14	17 ± 3	–	–	≤2.5(10)	–	–	−18.1	4.0	7.0(10)	3.0–6.0	5.0–9.0(10)
			−8.1	2.2	2.0(12)	1.2–2.8	1.5–20(12)	−8.1	1.5	6.0(10)	1.0–3.5	0.5–1.0(11)
			−3.1	2.0	2.5(11)	≤3.0	1.5–3.0(11)	−3.1	3.0	4.0(10)	2.5–5.0	3.0–6.0(10)
ρ Sco	≤5.0	≤1.5	–	–	≤2.5(10)	–	–	–	–	≤1.6(10)	–	–

(*continued*)

Table 2 (continued)

Star	w_λ(Na I)	w_λ(Ca II)	Na I components					Ca II components				
			v_{lsr}	b	N	Δb	ΔN	v_{lsr}	b	N	Δb	ΔN
48 Lib	211 ± 17	33 ± 20	−12.6	0.8	1.0(12)	0.4–1.0	0.8–10(12)	−13.1	–	9.6(10)	–	0.7–1.2(11)
			−4.0	0.8	3.5(12)	0.4–1.0	0.2–10(13)	−4.1	–	≤1.2(11)	–	–
			+2.1	1.2	1.8(12)	0.4–2.0	0.1–15(13)	+1.9	–	–	–	0.4–3.0(11)
143699	≤5.0	14 ± 2	–	–	≤2.5(10)	–	–	−12.5	10.0	1.6(11)	8.0–12.0	1.1–2.0(11)
ω^1 Sco	229 ± 19	36 ± 5	−13.4	0.8	2.6(11)	≤1.2	2.2–4.0(11)	−13.4	2.0	8.0(10)	1.0–3.5	0.6–1.1(11)
			−5.4	2.5	2.0(11)	1.5–3.0	1.5–2.6(11)	–	–	≤4.2(10)	–	–
			+1.6	3.0	2.5(12)	1.5–3.5	0.2–30(13)	+1.1	2.5	4.0(11)	1.5–3.0	3.5–4.5(11)
χ Oph	260 ± 22	81 ± 7	−14.2	3.0	1.2(11)	1.0–5.0	0.8–2.0(11)	−15.2	3.2	2.6(11)	2.8–4.0	2.2–3.0(11)
			−7.7	1.8	5.4(11)	≤2.5	0.4–10(12)	−7.7	4.0	1.4(11)	2.0–7.0	1.0–2.2(11)
			+1.8	3.2	2.6(12)	1.5–3.5	0.23–50(13)	+0.8	2.0	6.5(11)	1.0–2.5	5.5–8.0(11)
			–	–	≤7.0(10)	–	–	+6.3	1.5	4.0(10)	≤3.0	2.0–8.0(10)
148703	152 ± 13	51 ± 6	–	–	≤2.0(10)	–	–	−17.6	4.0	8.0(10)	3.0–7.0	0.6–1.2(11)
			−9.6	1.6	1.2(11)	≤2.5	0.9–1.3(11)	−10.6	2.5	1.8(11)	1.0–3.0	1.2–2.0(11)
			−1.1	2.0	1.0(12)	≤2.5	0.8–200(12)	−2.1	3.5	1.5(11)	2.0–4.5	1.1–1.8(11)
			+3.4	2.0	1.5(11)	≤3.0	1.0–3.0(11)	+2.4	3.0	3.0(10)	–	1.0–5.0(10)
			–	–	≤9.0(10)	–	–	+7.4	2.0	1.5(11)	≤3.0	1.2–3.0(11)
			+12.4	5.0	8.0(10)	4.0–6.0	0.6–1.0(11)	–	–	≤5.0(10)	–	–
μ^1 Sco	9.5 ± 2.1	6.9 ± 1.7	–	–	≤1.0(10)	–	–	−20.2	3.0	3.0(10)	1.0–4.0	2.0–4.0(10)
			–	–	≤1.0(10)	–	–	−10.7	1.0	4.0(10)	≤2.0	3.0–5.0(10)
			+0.5	0.8	7.0(10)	≤1.0	6.0–7.5(10)	–	–	≤2.1(10)	–	–
θ Oph	87 ± 9	38 ± 4	–	–	≤3.5(10)	–	–	−13.8	4.0	1.6(11)	3.0–5.0	1.2–1.9(11)
			−8.1	3.5	9.0(10)	2.0–5.0	0.7–1.1(11)	−8.1	1.8	1.2(11)	≤2.5	1.0–4.0(11)
			−0.1	1.3	9.0(11)	≤2.0	0.6–100(12)	−0.1	0.8	1.6(11)	≤1.0	1.4–5.0(11)
			–	–	≤2.6(10)	–	–	+20.7	1.5	3.0(10)	≤2.0	2.0–4.0(10)

for Ca K (Morton & Smith 1973). The Na D2 line consists of two unresolved hyperfine components (separated by 0.97 km s^{-1} in velocity units) and this structure has been included in the line profile modelling.

Many of the velocity components were found to be essentially unresolved, and an upper limit to b is therefore given in Table 2. Since the line saturates at a lower column density for smaller b, it is necessary to estimate a lower limit to b in order to obtain an upper limit to the column density for the unresolved lines. With one or two exceptions, the small stellar reddenings, and low interstellar column densities, suggest that the clouds observed here have properties similar to the 'median' H I cloud discussed by Kulkarni & Heiles (1987), i.e. $T \sim 115$ K and $E_{B-V} \sim 0.02$ mag. A temperature of 115 K corresponds to a b value (for Na) of 0.29 km s^{-1}. Since any bulk motions ('turbulence') in the cloud will increase b, we will adopt 0.3 km s^{-1} as a lower limit to the sodium velocity dispersion. This limit is consistent with the b values found by the very high-resolution observations of diffuse clouds by Blades et al. (1980). Since, in the absence of turbulence, $b_{Na}/b_{Ca} = 1.3$, we will assume a minimum b value for calcium of 0.23 km s^{-1}. These are the b values used to obtain the column density upper limits given in Table 2 for unresolved lines.

For some of the stronger unresolved lines, it was possible to obtain a lower limit to b (and hence upper limit to N) from the fact than none of the observed lines exhibit damping wings. For example, in the case of the strongest Na component observed towards 1 Sco it was found that, with $b = 0.3$ km s^{-1}, the column density required to match the central depth of the line was so large ($5\,10^{14}$ cm^{-2}) that the model profile developed prominent wings, which do not occur in the observed spectrum. As a result, it was possible to infer a minimum b value of 0.6 km s^{-1} (i.e. $b = 0.6$ km s^{-1} for each unresolved hyperfine component), and hence further constrain the column density. Similarly, the b values of the three Na components observed towards 48 Lib were found to be greater than 0.4 km s^{-1}.

Finally, we note that previous work with this spectrograph (e.g. Crawford et al. 1989) found evidence for a zero level error corresponding to between about 2% and 4% of the continuum intensity (presumed to be due to scattered light). Since most of the lines observed here are fairly weak, a zero level error of this magnitude will only have a small effect on the derived column densities ($\lesssim 10\%$, which is much less than that due to uncertainties in the b values). However, for lines which would actually reach zero intensity in the absence of a zero level error (such as the strongest Na components towards ω^1 Sco and χ Oph) this may result in a column density underestimate of more than an order of magnitude; for lines with a core residual intensity of about 10% (e.g. the Na lines towards 1 Sco and 2 Sco) the corresponding column density error was found to be about a factor of two. These uncertainties have been included in the column density limits listed in Table 2.

Table 3. Comparison between the equivalent widths obtained here and those given by Hobbs (1974, 1978, 1984). Units are mÅ

HD	Name	Na I D2		Ca II K	
		Hobbs	Here	Hobbs	Here
141637	1 Sco	225	218 ± 18	–	–
144470	ω^1 Sco	240	229 ± 19	37	36 ± 5
148184	χ Oph	295	260 ± 22	–	–
151890	μ^1 Sco	–	–	12	7 ± 2
157056	θ Oph	–	–	≤30	38 ± 4

5. Comparison with previous results

Very high-resolution (0.5 km s^{-1}) interstellar spectra for five of the stars discussed here (1 Sco, ω^1 Sco, χ Oph, μ^1 Sco and θ Oph) have previously been presented by Hobbs (1969, 1974, 1978 and 1984). In all cases the velocity structure found by Hobbs agrees well with that found here, although his higher resolution enabled him to identify additional structure within the stronger lines towards 1 Sco, ω^1 Sco and χ Oph. The equivalent widths given by Hobbs (1974, 1978 and 1984) are also in good agreement with those obtained here; for convenience this comparison is made in Table 3. Note that although Hobbs (1978) only gives an upper limit for the interstellar Ca II lines towards θ Oph, they are clearly visible superimposed on the broad stellar line in his Fig. 5.

Of particular interest is the fact that Hobbs' (1984) spectrum confirms the reality of the weak Ca II components found at $v_{lsr} = -20.2$ and -10.7 km s^{-1} (i.e. -27 and -17.5 km s^{-1} heliocentric) towards μ^1 Sco. This is of interest because these do not correspond to the weak Na D_2 component found at $+0.5$ km s^{-1} (-6.3 km s^{-1}, heliocentric) towards this star, a component whose reality is itself confirmed by Hobbs' (1978) Na D_1 spectrum. Thus Hobbs' data confirm the existence of all three weak components towards μ^1 Sco, although it seems clear that the $+0.5$ km s^{-1} component must have a higher Na I/Ca II ratio than the other two. Also of interest is the fact that Hobbs' (1978) Ca II spectrum of θ Oph does indicate weak absorption at $v_{lsr} \sim 21$ km s^{-1} ($+10$ km s^{-1}, heliocentric) confirming the reality of the weak line listed at $+20.7$ km s^{-1} in Table 2. The fact that Hobbs' data has confirmed the reality of these weak lines lends support to those of similar strength found towards other stars in the present sample (e.g. Ca II towards ρ Sco, δ Cru, ϵ Cen, μ Cen ϕ Cen, λ Lup, and 2 Sco).

Finally, we note that Hobbs (1969, 1974) has presented Na I and Ca II absorption line data for seven members of the US subgroup that were not observed here (namely, π Sco, δ Sco, β^1 Sco, ν Sco, σ Sco, τ Sco and ζ Oph). These stars exhibit velocity structure similar to that found for the US stars observed here, i.e. strong absorption lines close to zero velocity in the LSR, and weaker absorption blue shifted by up to 15 km s^{-1}.

6. The velocity structure

It is well known (e.g. Crutcher 1982; Frisch & York 1986) that nearby interstellar clouds observed in the direction of Sco-Cen ($270° \lesssim l \lesssim 360°$) generally have negative radial velocities with respect to the local standard of rest. This tendency is very clearly borne out by the present data: out of the 58 identified velocity components (towards 23 stars) 46 (or 79%) were found to have negative LSR velocities. Although negative velocities are expected in this quadrant owing to differential galactic rotation, for nearby stars this effect is small. Galactic rotation results in the most negative velocities at $l = 315°$, but at a distance of 150 pc this amounts only -2.0 km s^{-1} (assuming an Oort constant of 13 km s^{-1} kpc^{-1}, Fich et al. 1989). Most of the velocities observed towards nearby stars in this quadrant are significantly more negative than this, and it is generally accepted that they reflect a general outflow of material from the Sco-Cen association. This interpretation is fully consistent with observations of outflows from many other OB associations (e.g. Munch 1957; Walborn & Hesser 1975; Cowie et al. 1979, Phillips & Gondhalekar 1981; Phillips et al. 1984; Crawford et al. 1989).

We will now discuss the presently observed interstellar cloud velocities from the point of view of two different possible descriptions of this flow of material towards the sun. These are, firstly, an assumption that the velocities can be described by a single interstellar wind vector, and, secondly, that they can be described in terms of an expanding shell centered on the Sco-Cen association.

6.1. *A local interstellar wind vector*

If the sun is embedded within a coherently moving interstellar wind from a direction (l_w, b_w) with velocity v_w, the component of v_w in any direction (l, b) is given by

$$v = v_w\{\sin b \sin b_w + \cos b \cos b_w \cos(l - l_w)\}, \quad (1)$$

where the term in curly brackets is just the cosine of the angle between (l, b) and (l_w, b_w). Crutcher (1982) performed a least square fit to this equation for the interstellar cloud velocities observed towards six nearby ($d \leq 100$ pc) stars, obtaining a local (LSR) interstellar flow vector of $(l_w, b_w, v_w) = (345°, -10°, -15$ km s$^{-1})$. Crutcher then went on to show that this vector was generally consistent with the velocities of interstellar components towards an additional 45 more distant stars. Frisch & York (1986) have performed a similar analysis of components towards 21 stars with $d \lesssim 100$ pc, and obtained a similar velocity vector $[(l_w, b_w, v_w) = (354°, +3°, -12$ km s$^{-1})]$. The latter vector is in slightly better agreement with the velocities observed here than the former (the rms residuals are 10.5 and 9.1 km s^{-1}, respectively), although it is clearly not very satisfactory. A least-square fit to the velocities of all the components identified in the present data yields a best fit LSR vector of $(l_w, b_w, v_w) = (289°, +42°, -9$ km s$^{-1})$, with an rms residual of 8 km s^{-1}. Interestingly, however, it was found that a very much better fit was obtained by considering only those components that were positively identified in both Na I and Ca II; in this case a least-square fit yielded the vector $(301°, +59°, -9$ km s$^{-1})$, with an rms residual of only 5 km s^{-1}.

Figure 3 shows the LSR velocities of the components identified in the present work, plotted as a function of galactic longitude. In this figure, the components observed in both Na I and Ca II are represented by solid dots, whereas those observed in only one or the other are represented by open symbols. The best fitting velocity vector (all components) is indicated in Fig. 3 by the solid curve, where the predicted velocity has been referred to the plane of Gould's Belt. [Since the predicted velocity depends on both l and b it is necessary to assume some relation between them for

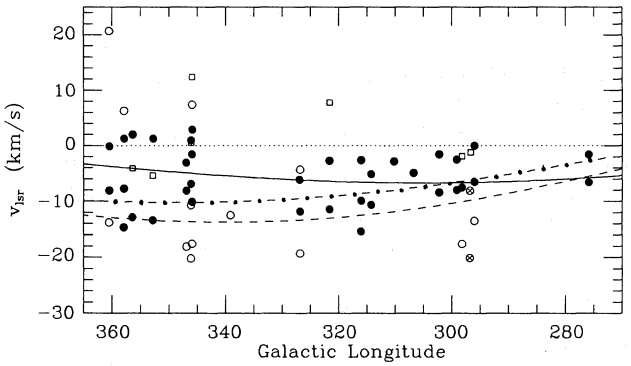

Fig. 3. The LSR velocities of the observed components plotted as a function of galactic longitude. Components identified in both Na I and Ca II are represented by *solid circles*, components identified in Ca II only are represented by *open circles*, and components identified in Na I only are represented by *open squares*. The Ca II components observed towards ρ Cen are marked by $\otimes$ *symbols*; as no Na I spectrum was obtained for this star, the fact that only Ca II data are presented here does not imply a low Na I/Ca II ratio. Note that the majority of the components have negative LSR velocities, and that the velocity scatter is greatest for components observed in only one species. The *solid line* shows the velocity (referred to the plane of Gould's Belt) predicted by the best-fitting vector solution discussed in the text (Sect. 6.1). The *dashed curve* shows the velocities predicted by the vector obtained by Crutcher (1982), and the *dot-dashed curve* shows the velocities predicted by vector *A* of Lallement et al. (1986); see text for discussion

the construction of the figure; as Sco-Cen lies along Gould's Belt (Fig. 1b) this is a better approximation than assuming that the stars lie in the galactic plane. In the least squares fitting procedure this assumption was *not* made, *l*, *b* and *v* all being treated as free parameters.] The greater scatter about the best fitting curve of components observed in only one species is readily apparent from Fig. 3. Clouds with anomalous velocities are generally found to have low Na I/Ca II ratios (e.g. Routly & Spitzer 1952; Siluk & Silk 1974; Crawford et al. 1989), and some of the observed scatter may be due to this effect. The Na I/Ca II ratios are considered in more detail in Sect. 7.

Lallement et al. (1986) have carried out a search for Ca II components arising in the local interstellar medium, and found evidence for four separate coherent motions within the distance range 5 to 100 pc from the sun. The corresponding vectors (labelled *A*, *O*, *P* and *I*) are listed in Table 2 of their paper. The velocities predicted by their vector *A* are indicated in Fig. 3 (dash-dot curve) for the longitude range of interest here, and it will be seen that for the longitude range $270° \lesssim l \lesssim 320°$ it predicts velocities close to the best-fitting vector obtained here. At greater longitudes, it predicts velocities that are more negative than the average, but which are nevertheless consistent with many observed components. In fact, of the 23 stars with components identified in Table 2, 20 (87%) have absorption components within 3 km s^{-1} of the velocity predicted by Lallement et al.'s vector *A*. The other vectors identified by Lallement et al. (1986) predict more negative velocities, and are not consistent with the majority of the components observed here, although they are generally consistent with those having the most negative velocities. The range of velocities predicted by the vectors of Lallement et al. (1986), for each of the observed stars, is indicated in Fig. 2 (see also Fig. 6a).

Crutcher's (1982) vector is also indicated in Fig. 3. It will be seen that this predicts velocities more negative than vector *A*, but, as noted by Lallement et al., may be interpreted as an average of the four separate vectors identified by them. The vector determined by Frisch & York (1986) yields essentially the same velocities as Lallement et al.'s vector *A* for $270 \lesssim l \lesssim 300$, and lies between vector *A* and Crutcher's vector for the remainder of the longitude range considered here.

6.2. *An expanding shell centred on the Sco-Cen association*

The Sco-Cen association is known to be surrounded by loops of neutral hydrogen (see, for example, the photographic representation of the galactic H I distribution presented by Colomb et al. 1980), and it has been suggested by Weaver (1979) that these represent the surface of an expanding bubble centred on the Sco-Cen association. According to this view, the expansion is driven by mass loss from the most massive association members, although there is evidence that the original wind-driven bubble has been subsequently modified by at least one supernova event (see Cox & Reynolds 1987 for a recent review).

The H I shells associated with the Sco-Cen association have recently been discussed by de Geus (1991), who presented evidence for three shells, one associated with each of the three association subgroups. For convenience some of the shell parameters listed by de Geus are reproduced in Table 4. All quantities except the distance, *R*, to the shell centre have been taken from Table 1 of de Geus (1991); the values adopted for *R* are those obtained by Jones (1971) for the distance to each subgroup. Note that de Geus found no evidence of expansion for the LCC shell. These shells are indicated by circles of the appropriate size in Figs. 1a and 1b. It is clear that the UCL shell dominates this region of space and, if even approximately circular, encompasses both the other two shells and the 'wall' of local dark clouds.

If the negative absorption line velocities observed in this quadrant are due to an expanding shell centred on the Sco-Cen as-

Table 4. Parameters describing the H I shells associated with the Sco-Cen association: l_0, b_0 are the coordinates of the shell centre; v_0 is the shell expansion velocity; r_s is the shell radius; *R* is the distance to the shell centre. All values have been taken from Table 1 of de Geus (1991), except the values of *R* which are from Jones (1971)

Subgroup	l_0	b_0	v_0 (km s^{-1})	r_s (pc)	*R* (pc)
LCC	297 ± 5	15 ± 5	–	35 ± 10	130 ± 24
UCL	320 ± 3	10 ± 3	10 ± 2	110 ± 10	140 ± 20
US	347 ± 2	21 ± 2	10 ± 2	40 ± 4	160 ± 22

sociation then, owing to the proximity of this shell (cf. Fig. 1a), we might expect an expanding shell model to be in better agreement with the observations than the assumption of a single flow vector such as that considered by Crutcher (1982) and Frisch & York (1986). The radial velocity observed for a point (l, b) on the surface of sphere of radius r_s, centred a distance R from the sun at (l_0, b_0), is given (e.g. Cleary 1977) by:

$$v = \pm\frac{v_0}{r_s}\sqrt{R^2(\cos^2\theta - 1) + r_s^2}, \qquad (2)$$

where θ is the angle between (l, b) and (l_0, b_0), and $\cos\theta$ is given by the term in curly brackets in Eq. 1 (substituting l_0, b_0 for l_w, b_w).

The velocity, v, predicted by Eq. 2 for any direction (l, b) intersecting the surface of the sphere was found to depend most sensitively on v_0, and to be relatively insensitive to the other parameters (within the range of uncertainties estimated by de Geus (1991)). The value of v_0 that yielded the best fit to the observed components was found to have $v_0 = 7\,\mathrm{km\,s^{-1}}$, somewhat less than the value of $10 \pm 2\,\mathrm{km\,s^{-1}}$ quoted by de Geus (1991) for the UCL shell. This value was found to be essentially independent of whether all the components were included, or only those observed in both Na I and Ca II, although the rms residual is much larger in the former case ($7.9\,\mathrm{km\,s^{-1}}$) than in the latter ($4.9\,\mathrm{km\,s^{-1}}$). Also, we note that, although $v_0 = 7\,\mathrm{km\,s^{-1}}$ does minimise the residuals, these are only marginally larger if de Geus's value of $10\,\mathrm{km\,s^{-1}}$ is adopted (the rms residuals in this case being 8.2 and $5.5\,\mathrm{km\,s^{-1}}$ for the two cases considered above).

The velocities predicted by an expanding shell with $v_0 = 7\,\mathrm{km\,s^{-1}}$, with other parameters as given in Table 4 for the UCL shell (and again referred to the plane of Gould's Belt), are compared with the observed interstellar cloud velocities in Fig. 4. Comparison between Figs. 3 and 4 shows that, over most of the longitude range considered, the best fitting shell model agrees very closely with the best fitting interstellar wind vector, although a shell model is to be preferred on physical grounds. Having determined the best-fitting single shell solution for the observed components, we now examine the evidence for the three separate shells listed by de Geus (1991).

6.2.1. The UCL shell

All of the stars observed here lie within the longitude range covered by the UCL shell (Fig. 1a), and would therefore be expected to exhibit components arising in this shell. As most of the stars have several velocity components, not all of which are necessarily associated with the UCL shell, it is of interest to determine whether the majority have at least one component at the predicted velocity. By determining the velocities predicted by a range of shell models, it was found that the residuals between the model and the component *towards each star* with a velocity closest to that of the model, was minimised for $v_0 = 9\,\mathrm{km\,s^{-1}}$. The rms residual (considering one component per star) for this value of v_0 was $2.8\,\mathrm{km\,s^{-1}}$. As before, this result was found to be more sensitive to v_0 than to the other shell parameters, although a variation in v_0 of $\pm 2\,\mathrm{km\,s^{-1}}$ results is only a small ($\lesssim 0.4\,\mathrm{km\,s^{-1}}$) increase in the rms residual. The velocities predicted by the $v_0 = 9\,\mathrm{km\,s^{-1}}$ shell are shown in Fig. 5a, which also marks those components (one per star) with velocities closest to those predicted by this model. The Na I/Ca II ratios of these components are shown in Fig. 5b, and will be discussed in Sect. 7.3. For comparison, the velocities and Na I/Ca II ratios of the remaining components (i.e. those not identified with the $9\,\mathrm{km\,s^{-1}}$ UCL shell) are shown in Fig. 6.

6.2.2. The US shell

Of the stars observed here, eight (HD 141637 to HD 148703 inclusive in Table 1) would be expected to sample the US shell in addition to the UCL shell (assuming the shell parameters given by de Geus 1991). It turns out that the radial velocities predicted

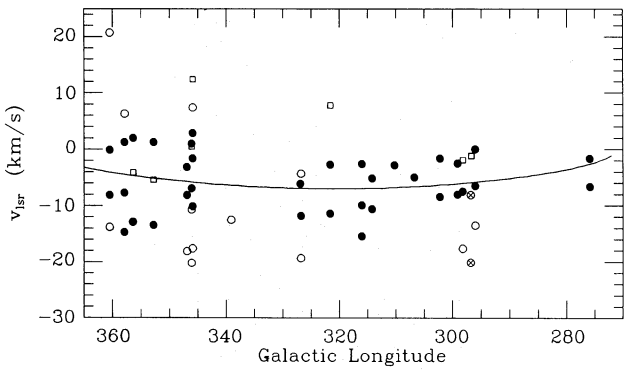

Fig. 4. The velocity predicted by the best-fitting shell model ($v_0 = 7\,\mathrm{km\,s^{-1}}$, other parameters as given in Table 4 for the UCL shell), compared with the observed velocities. (*Symbols* as for Fig. 3.)

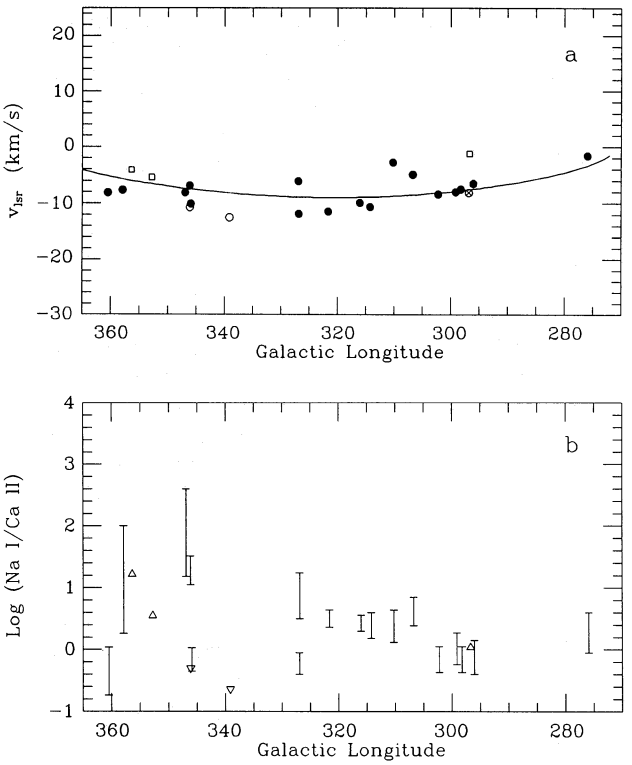

Fig. 5. a The velocity predicted by the best-fitting UCL shell model ($v_0 = 9\,\mathrm{km\,s^{-1}}$) obtained under the assumption that only one component per star arises in this shell; the *dots* indicate the observed velocities of these components. (*Symbols* as for Fig. 3.). **b** Na I/Ca II ratios of these 'UCL shell' components. *Error bars* indicate the extreme limits to this ratio implied by the maximum and minimum column densities given for each component in Table 2. Upper and lower limits are indicated by *open triangles* pointing in the appropriate direction

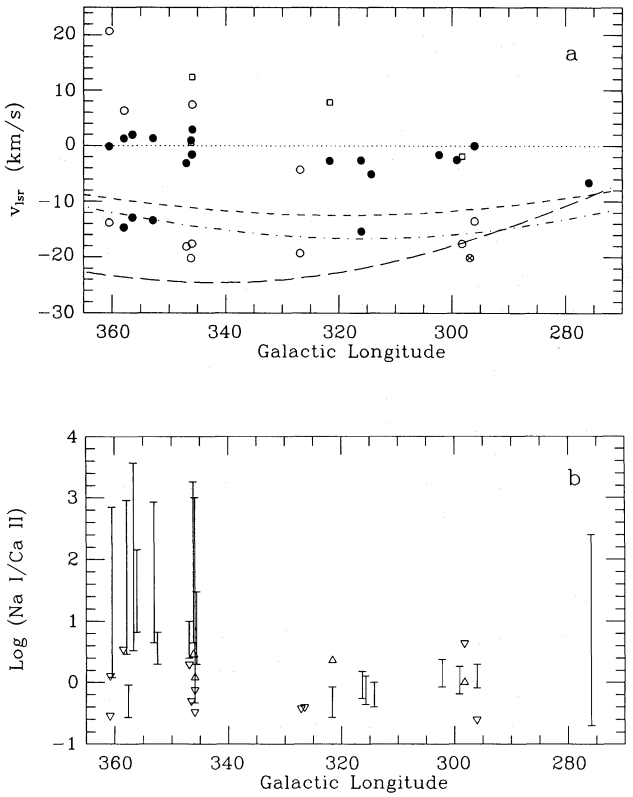

Fig. 6. a As for Fig. 3, but with the 'UCL shell' components (i.e. those shown in Fig. 5a) excluded. The different classes of component that may be identified in this figure are discussed in the text. The *short-dashed, dot-dashed* and *long-dashed curves* indicate the velocities predicted by vectors *O, I* and *P*, respectively, of Lallement et al. (1986). **b** Na I/Ca II ratios of the components shown in **a**. (*Symbols* as for Fig. 5b)

for the US shell differ by $\lesssim 3\,\mathrm{km\,s^{-1}}$ from that predicted for the UCL shell, which is not sufficient to distinguish unambiguously between them. However, since none of these seven stars were found to have two appropriately spaced components, and for all but one (χ Oph) the observed velocities are in better agreement with those predicted by the UCL shell, there is no convincing evidence in the present velocity data for components arising in the US shell. However, circumstantial evidence that some of the components observed towards the US subgroup, and identified above with the UCL shell, may nevertheless arise in the US shell will be discussed in Sect. 7.3.

6.2.3. The LCC shell

Given the shell parameters listed in Table 4, the lines of sight to δ Cen, δ Cru, σ Cen, HD 110956, and ϵ Cen would be expected to intercept the LCC shell in addition to the UCL shell. The star ρ Cen also lies in this direction, but the nominal distance to this star (83 pc) places it in the foreground (cf. Fig. 1a). All five of these stars have components with low (negative) LSR velocities ($-3 \lesssim v_{lsr} \lesssim 0\,\mathrm{km\,s^{-1}}$) which were not identified with UCL shell. [Note that only one component was observed towards ϵ Cen, and this component was therefore included in the fitting to the UCL shell described above. However, the low velocity of this component ($v_{lsr} = -2.8\,\mathrm{km\,s^{-1}}$) is more consistent with it belonging to the group of components discussed here than with it being identified with the UCL shell.]

In his analysis, de Geus (1991) was unable to find any evidence for expansion of the LCC shell. However, a small expansion velocity ($\sim 2\,\mathrm{km\,s^{-1}}$) would be consistent with the five components discussed above arising in the LCC shell. Moreover, if the LCC shell radius were as large as 45 pc (i.e. at the upper end of the range estimated by de Geus) an expansion velocity of $\sim 2\,\mathrm{km\,s^{-1}}$ would also account for the low negative velocity components observed towards ϕ Cen and μ Cen.

The distances adopted for some of these stars places them beyond the far side of the LCC shell (cf. Fig. 1a). However, no positive velocity components were identified in this longitude range, so there is no evidence in the present data for components arising in the receding part of this shell. This observation suggests either that the LCC shell lies further from the sun than estimated by de Geus (1991), or has a larger radius.

7. Discussion

In this section we first give a general discussion of the Na I/Ca II ratios, and then a more detailed discussion of the different classes of component which may be identified in the velocity data.

7.1. *General discussion of the* Na I/Ca II *ratios*

In Fig. 7 we plot the Na I/Ca II ratios of the observed components as a function of velocity with respect to the LSR. For components observed in both Na I and Ca II, the vertical bars mark the extreme upper and lower limits that this ratio may take (based on the maximum and minimum column densities given for each component in Table 2); upper and lower limits are indicated by open triangles pointing in the appropriate direction. Within the velocity range $-14 \lesssim v_{lsr} \lesssim +4\,\mathrm{km\,s^{-1}}$, we see that there is a large spread in the Na I/Ca II ratios. Included within this velocity range are components with well defined Na I/Ca II ratios (some with numerical values as low as ~ 0.2, but others as high as ~ 10), as well as components with very poorly determined ratios (owing to saturation in the Na lines), but for which the Na I/Ca II ratio may reach values as high as 10^3. At more negative velocities we find only upper limits to the Na I/Ca II ratio, while at more positive velocities we find three upper and two lower limits. The upper limits at both negative and positive velocity extremes are as expected from the Routly-Spitzer effect [i.e. high velocity clouds have low Na I/Ca II ratios; Routly & Spitzer (1952), Siluk & Silk (1974)]. The two lower limits found in the positive velocity region

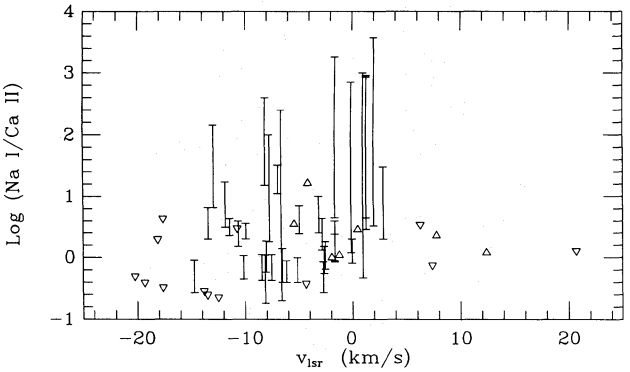

Fig. 7. Na I/Ca II ratios for all identified components plotted as a function of LSR velocity

are somewhat surprising from this point of view, but are nevertheless consistent with lower Na I/Ca II ratios than found for the strong components near $v_{lsr} = 0\,km\,s^{-1}$.

Jura (1976) has argued that variations in the Na I/Ca II ratio for different clouds are primarily due to variations in the gas-phase abundance of calcium, since the sodium depletion is known to be approximately constant in diffuse interstellar clouds (Phillips et al. 1984; Jura 1975). The Na I/Ca II ratio is larger in denser clouds owing to the increasing adsorption of calcium onto the grain surfaces. The Routly-Spitzer effect may then be attributed to the removal of adsorbed calcium atoms from grain surfaces by interstellar shock waves in clouds with high peculiar velocities (Barlow & Silk 1977; Barlow 1978). A somewhat more detailed discussion of this mechanism has been given by Crawford et al. (1989).

7.2. *Stars with no observed absorption components*

Five stars in the present sample were found not to have identifiable absorption components. For two of these (γ Lup and HD 138769) only the spectral region of one line was observed (Na I for γ Lup and Ca II for HD 138769), so the non-detections may just reflect peculiar Na I/Ca II ratios towards these stars. For the other three stars (o Lup, β Lup and ρ Sco) both spectral regions were observed, so the low upper limits obtained suggest that the lines of sight towards these stars are essentially devoid of absorbing clouds. Note that none of these stars are among the closest to the sun, and that all are well within the interior of the UCL shell (Fig. 1a). These observations therefore imply that the interior of the shell is largely empty, and that the distribution of clouds around the surface of the shell is patchy.

7.3. *The UCL shell components*

In this section we will consider those components (one per star) that have velocities closest to those predicted by a shell expanding at a velocity of $9\,km\,s^{-1}$ and centred on the UCL subgroup of the association (i.e. those components plotted in Fig. 5a). These will be referred to as the 'UCL shell' components. Note, however, that although the $9\,km\,s^{-1}$ shell gave the best fit on the *assumption* that one component per star arises in this shell, the fact that the shell has holes in it (Sect. 7.2), and that a reasonable shell model can be fitted to *all* the observed components (albeit with a greater scatter), means that this assumption must be tentative.

Twenty out of the 23 stars with velocity components given in Table 2 (87%), were found to have a component within $3.5\,km\,s^{-1}$ of the value predicted for a shell expanding at $9\,km\,s^{-1}$ (and with the other parameters as given in Table 4). An expansion velocity of $9\,km\,s^{-1}$ is well within the uncertainty given by de Geus (1991) for the UCL shell. As the velocity at each point on the surface of this shell will depend on the ambient density of the interstellar medium, small differences between the observed and predicted velocities are to be expected. Thus, for the great majority of the stars observed, the present observations are consistent with at least one component per star arising in the UCL shell.

Figure 5b shows the Na I/Ca II ratios of those components with velocities closest to those predicted by this shell. As explained in Sect. 6.2.1, one component per star has been included in this plot. It will be seen that most of these components have Na I/Ca II ratios in the range 0.2 to about 6, which is essentially the same as the range found for the expanding shell centred on the Scorpius OB1 association by Crawford et al. (1989; their Fig. 7). These ratios are therefore consistent with the view that in shell components calcium has been removed from grain surfaces, leading to a relatively low Na I/Ca II ratio.

It is noteworthy that the four UCL shell components with Na I/Ca II ratios significantly above this range (i.e. those towards 1 Sco, 2 Sco, 48 Lib and χ Oph) all lie towards the US subgroup, where the quantity of foreground interstellar matter is known to be enhanced above the Sco-Cen average (e.g. de Geus et al. 1990), owing to the presence of the ρ Oph and Lupus dark clouds in this direction. Note, however, that the UCL shell surface lies much closer to the sun than the US dark clouds, and it is therefore difficult to understand why gas associated with these clouds should have velocities predicted by this shell. As noted in Sect. 6.2.2, the velocities predicted by the US shell are not significantly different from those of the UCL shell in this direction, and as the US shell lies close to the Lupus and ρ Oph dark clouds (Fig. 1a), it may be that these components actually arise in dense gas associated with the US shell. This would then account for their higher Na I/Ca II ratios. Note that although the distances to 1 Sco and 2 Sco given by de Geus et al. (1989) place these stars in front of the US shell, the fact that they have significantly greater reddenings than the other stars (Table 1) suggests that these distances may have been underestimated. In this respect we note that Paresce (1984) adopted a distance of 232 pc for 1 Sco, which is more consistent with these observations.

7.4. *Low velocity components towards the US subgroup*

In the longitude range $345° \lesssim l \lesssim 360°$, i.e. towards stars belonging to the US subgroup, there are a number of low velocity ($-4 \lesssim v_{lsr} \lesssim +4\,km\,s^{-1}$) components with generally strong Na I lines (cf. Fig. 2), and large Na I/Ca II ratios (Fig. 6b). Comparison with Fig. 7 of Crawford et al. (1989) shows that these components have Na I/Ca II ratios consistent with an origin in dense foreground clouds in which much of the calcium has condensed onto grain surfaces. A high density in these clouds is consistent with the proximity of the ρ Oph and Lupus dark clouds to the line of sight, and the extensive CO emission detected in this region by de Geus et al. (1990). The fact that these components are at rest in the LSR suggests that they have not been affected by the Sco-Cen shell. This is consistent both with these clouds having large masses, and also with their location *inside* the UCL shell (cf. Fig. 1a, from which we see that any impetus given to these clouds from the direction of the shell centre would have largely been tangential to the line of sight).

Cappa de Nicolau & Pöppel (1986) have carried out a detailed study of the H I profiles towards the US subgroup, and it is of interest to compare their observations with the present data. The strongest, and most extensive, component identified by Cappa de Nicolau & Pöppel (1986) was their component *G*, which was found to occupy the velocity range $-0.5 \lesssim v_{lsr} \lesssim +2.5\,km\,s^{-1}$. Of the six stars in the present sample which lie in the region studied by Cappa de Nicolau & Pöppel (1 Sco, 2 Sco, ρ Sco, ω^1 Sco, 48 Lib and χ Oph) all except 2 Sco and ρ Sco were found to have components in the range covered by component *G*. The components at this velocity in the present data (indicated by solid circles in Fig. 2) were all found to have strong Na I lines and large Na I/Ca II ratios. The non-detection of this component towards 2 Sco and ρ Sco is consistent with Cappa de Nicolau & Pöppel's observations, which show that these stars are located in an area

where emission by this component is relatively weak. Components with velocities consistent with component *G* can also be identified towards μ^1 Sco, HD 148703 and θ Oph, which lie within the longitude range considered by Cappa de Nicolau & Pöppel (1986). but at more negative galactic latitudes.

Thus we see that the low velocity, high Na I/Ca II ratio, clouds observed towards the US subgroup may be identified with Cappa de Nicolau & Pöppel's component *G*. The suggestion that these arise in relatively dense diffuse clouds associated with the nearby dark clouds is supported by the detection of interstellar CH in this component towards ω^1 Sco and χ Oph by Danks et al. (1984), and C_2 towards χ Oph by van Dishoeck & de Zeeuw (1984). From their analysis of the rotational excitation of C_2, van Dishoeck & de Zeeuw found the kinetic temperature in this component towards χ Oph to lie between 25 and 70 K, with a hydrogen number density between 150 and 270 cm^{-3}. Note that the detection of this component towards 1 Sco, HD 148703, and θ Oph strongly suggests that the distances to these stars have been underestimated and that, in addition to 48 Lib, ω^1 Sco and χ Oph, these stars also are more distant than the dark clouds.

7.5. *Low velocity components in the range* $295° \lesssim l \lesssim 325°$

In the longitude range $295° \lesssim l \lesssim 325°$ there are several components with LSR velocities which are small but clearly negative ($-4 \gtrsim v_{lsr} \gtrsim 0\,km\,s^{-1}$). Unlike the components towards Upper Scorpius, however, the Na I/Ca II ratios of these components are not distinguishable from those of the UCL shell components. These are the components discussed in Section 6.2.3 as possibly arising in the LCC shell. Since H I emission in this longitude range has been attributed to a LCC shell (de Geus 1991), it is not unreasonable to expect corresponding Na I and Ca II absorption lines. If these components do arise in an LCC shell they imply an expansion velocity of $\sim 2\,km\,s^{-1}$.

7.6. *Components with anomalous negative velocities*

Figure 6a also shows the velocities predicted by the vectors *O*, *P* and *I* identified by Lallement et al. (1986) in the local interstellar medium, and it is clear that those components observed here which have velocities more negative than predicted by the UCL shell model are generally consistent with these flow vectors. The Na I/Ca II ratios are generally comparable with those of the shell components for where both species were identified (Fig. 6b), but note the relatively large number of upper limits (Fig. 6a; open circles) which suggest that these components may actually have much smaller Na I/Ca II ratios. This is consistent with an origin in a warm, low-density, medium (cf. the discussion in Section IV(d) of Crawford et al. 1989). The fact that Lallement et al. (1986) found similar components towards stars that are not only very nearby (within 20 pc), but distributed in all directions, suggests that this material envelopes the solar system. In the longitude range considered here, the velocities of these components are consistent with material flowing from Sco-Cen, but at higher velocities than the UCL shell. This local material therefore seems to form a high velocity precursor to the main Sco-Cen shell which has already overtaken the solar system, as suggested by Crutcher (1982).

7.7. *Components with significant positive velocities*

Figure 6a shows that there are five components with $v_{lsr} > 4\,km\,s^{-1}$, three of which were detected only in Ca II (towards χ Oph, HD 148703 and θ Oph), while two were detected only in Na I (towards HD 125823 and HD 148703). All but one occur towards stars of the US subgroup ($345° \lesssim l \lesssim 360°$). The Na I/Ca II ratios are all consistent with those of the shell and local components (the two lower limits to this ratio are still compatible with the highest upper limit).

Within the framework of an expanding shell model, positive velocities can arise only in the far side of the shell. Of these five stars, only χ Oph is placed beyond the far side of the UCL shell by the distances given by de Geus et al. (1989), and in this case the observed velocity agrees to within $1\,km\,s^{-1}$ of the predicted far side recession velocity. The nominal distances of the remaining four stars place them all within the UCL shell, although we saw above that there is convincing evidence for both HD 148703 and θ Oph actually lying at greater distances than indicated in Fig. 1a. Clearly, greater distances would make it easier to explain the presence of positive velocities towards these stars. Also, note that as the LCC and US shells exist *within* the UCL shell, these may give rise to red-shifted material in the interior of the latter; it may therefore not be necessary for stars to lie beyond the entire UCL shell in order for the lines of sight to intercept positive velocities.

In the context of positive velocities, it is of interest to note that observations of the Sco OB1 association (Crawford et al. 1989) revealed the presence of very low Na I/Ca II ratio components with velocities in the range $+10 \lesssim v_{lsr} \lesssim +28\,km\,s^{-1}$. The line of sight to the Sco OB1 association ($l = 343°, b = +1°$) passes through the UCL shell, and it is of interest to determine whether this shell can account for these components. In the direction of Sco OB1, the receding and approaching halves of the UCL shell would have velocities of $\pm 7.6\,km\,s^{-1}$ (taking $v_0 = 9\,km\,s^{-1}$). We see that these velocities are too small to account for the positive velocities observed towards Sco OB1. However, the very low Na I/Ca II ratios found for these components ($\lesssim 0.4$; cf. Fig. 7 of Crawford et al. 1989) suggests that these components may be related to the low density local interstellar components discussed in Sect. 7.6. As discussed in that section, these components appear to arise in a low density, high velocity precursor to the main Sco-Cen shell. If the *far side* of this shell has a similar precursor, low Na I/Ca II ratio components with LSR velocities of about $+15\,km\,s^{-1}$ would be expected, exactly as observed towards Sco OB1. Indeed, it may be that the large velocity range often found to be occupied by low Na I/Ca II material (discussed in Section IV(d) of Crawford et al. 1989) is due, at least in part, to low density gas preceding the expanding H I shells centred on OB associations.

8. Conclusions

The major conclusions of this study are as follows:

(1) The majority (79%) of the absorption components observed towards the Sco-Cen stars were found to have negative LSR radial velocities. This is in agreement with previous results (Crutcher 1982; Frisch & York 1986), and indicates that most of the diffuse clouds in this direction are moving outwards from the OB association.

(2) The best fitting interstellar flow vector (all components) was found to be described by $(l_0, b_0, v_0) = (289°, +42°, -9\,km\,s^{-1})$, with an rms dispersion of $8\,km\,s^{-1}$. A much better fit, $(301°, +59°, -9\,km\,s^{-1})$, was obtained by considering only components observed in both Na I and Ca II.

Neither of these vectors closely approximate the vectors found by Crutcher (1982), Frisch & York (1986) or Lallement et al. (1986).

(3) If it is assumed that the clouds exist on the surface of an expanding shell centred on the UCL subgroup of the association (de Geus 1991), then the best fitting expansion velocity (considering all components identified in both species) was found to be $7\,km\,s^{-1}$ with a rms residual of $4.9\,km\,s^{-1}$. Over most of the longitude/latitude range of interest the velocities predicted by this shell are virtually indistinguishable from those predicted by the best fitting flow vector discussed above (compare Figs. 3 and 4).

(4) At a somewhat deeper level of interpretation, if it is assumed that only one component per star is due to such a shell, the best fitting expansion velocity was found to be $9\,km\,s^{-1}$ with a rms residual of only $2.8\,km\,s^{-1}$ (Fig. 5). The Na I/Ca II ratios of these 'UCL shell' components are similar ($0.3 \lesssim$ Na I/Ca II $\lesssim 6$) to the values found by Crawford et al. (1989) for components associated with an expanding shell centred on the Sco OB1 association.

(5) If we remove these UCL shell components from the data set (cf. Fig. 6a), we are left with four other classes of component:

(i) Components essentially at rest with respect to the LSR which are associated with stars of the upper Scorpius subgroup, and which have large (potentially very large) Na I/Ca II ratios. These are thought to arise in relatively dense gas associated with the ρ Oph and Lupus dark clouds, and may be identified with component *G* of Cappa de Nicolau & Pöppel (1986).

(ii) Components with small but negative velocities, in the longitude range $295° \lesssim l \lesssim 325°$, and which have Na I/Ca II ratios indistinguishable from those of the shell components. If these are interpreted to arise in the LCC shell discussed by de Geus (1991) they imply an expansion velocity of $\sim 2\,km\,s^{-1}$ for this shell.

(iii) Components with velocities more negative than the UCL shell components. These components have generally lower Na I/Ca II ratios than the shell components (with a high proportion of upper limits), and velocities consistent with the local interstellar flow vectors identified by Lallement et al. (1986). These components are therefore identified with very local low density clouds, whose large negative velocities nevertheless also suggest outflow from Sco-Cen.

(iv) A small number of components with significant positive velocities, mostly observed towards the upper Scorpius subgroup. These may result from the receding part of the UCL and/or US shells, although such an interpretation would imply that the distances to HD 125823, HD 148703 and θ Oph are greater than those given by de Geus et al. (1989).

(6) It was suggested that the large velocity range often found to be occupied by low Na I/Ca II ratio material (discussed by Crawford et al. 1989) may be due to the low density, relatively high velocity, gas which appears to precede expanding H I shells.

Acknowledgements. The observations on which this paper is based were obtained while the author held a Royal Society Overseas Fellowship at Mt Stromlo. In addition to the Royal Society, I am grateful to the Director and staff of the Mt Stromlo and Siding Spring Observatories for their hospitality during this period, and to the Central Research Fund of the University of London for provision of a travel grant. I thank Dr. M.J. Barlow for helpful comments on an earlier draft of the manuscript.

References

Allen C.W., 1973, Astrophysical Quantities, 3rd ed., Athlone Press, London
Barlow M.J., 1978, MNRAS 182, 417
Barlow M.J., Silk J., 1977, ApJ 211, L83
Bertiau F.C., 1958, ApJ 128, 533
Blaauw A., 1964, ARA&A 2, 213
Blades J.C., Wynne-Jones I., Wayte R.C., 1980, MNRAS 193, 849
Cappa de Nicolau C.E., Pöppel W.G.L., 1986, A&A 164, 274
Cleary M.N., 1977, Ph.D. Thesis, Australian National University
Colomb F.R., Pöppel W.G.L., Heiles C., 1980, A&AS 40, 47
Cowie L.L., Songaila A., York D.G., 1979, ApJ 230, 469
Cox D.P., Reynolds R.J., 1987, ARA&A 25, 303
Crawford I.A., 1990, Observatory 110, 145
Crawford I.A., Barlow M.J., Blades J.C., 1989, ApJ 336, 212
Crawford I.A., Rees P.C.T., Diego F., 1987, Observatory 107, 147
Crutcher R.M., 1982, ApJ 254, 82
Dame T.M., Ungerechts H., Cohen R.S., de Geus E.J., Grenier I.A., May J., Murphy D.C., Nyman L.Å., Thaddeus P., 1987, ApJ 322, 706
Danks A.C., Federman S.R., Lambert D.L., 1984, A&A 130, 62
de Geus E.J., 1991, A&A (in press)
de Geus E.J., Bronfman L., Thaddeus P., 1990, A&A 231, 137
de Geus E.J., de Zeeuw P.T., Lub J., 1989, A&A 216, 44
Deutschman W.A., Davis R.J., Schild R.E., 1976, ApJS 30, 97
Fich M., Blitz L., Stark A.A., 1989, ApJ 342, 272
Franco G.A.P., 1990, A&A 227, 499
Frisch P.C., York D.G., 1986, in: The Galaxy and the Solar System, (eds.) R. Smoluchowski, J.N. Bahcall, M.S. Matthews, University of Arizona Press, Tucson, p. 83
Hobbs L.M., 1969, ApJ 157, 135
Hobbs L.M., 1973, ApJ 179, 823
Hobbs L.M., 1974, ApJ 191, 381
Hobbs L.M., 1978, ApJ 222, 491
Hobbs L.M., 1984, ApJS 56, 315
Hoffleit D., Jaschek C., 1982, The Bright Star Catalogue, 4th ed., Yale University Observatory, New Haven
Howarth I.D., Murray J., 1988, Starlink User Note, 50.11
Humphreys R.M., 1978, ApJS 38, 309
Jones D.H.P., 1971, MNRAS 152, 231
Jura M., 1975, ApJ 200, 415
Jura M., 1976, ApJ 206, 691
Kulkarni S.R., Heiles C., 1987, in: Interstellar Processes, (eds.) D.G. Hollenbach, H.A. Thronson, Reidel, Dordrecht, p. 87
Kurucz R.L., 1979, ApJS 40, 1
Lallement R., Vidal-Madjar A., Ferlet R., 1986, A&A 168, 225
Morton D.C., Smith W.H., 1973, ApJS 26, 333
Munch G., 1957, ApJ 125, 42
Paresce F., 1984, AJ 89, 1022
Phillips A.P., Gondhalekar P.M., 1981, MNRAS 196, 533
Phillips A.P., Pettini M., Gondhalekar P.M., 1984, MNRAS 206, 337
Phillips A.P., Welsh B.Y., Pettini M., 1984, MNRAS 206, 55
Routly P.M., Spitzer L., 1952, ApJ 115, 227
Siluk R.S., Silk J., 1974, ApJ 192, 51
Stothers R., Frogel J.A., 1974, AJ 79, 456
van Dishoeck E.F., de Zeeuw T., 1984, MNRAS 206, 383
Walborn N.R., Hesser J.E., 1975, ApJ 199, 535
Weaver H., 1979, IAU Symp. 84, 295